# Hydrodynamics of a Multiple Tidal Inlet System:
# Katama Bay, Martha's Vineyard, MA

by

## Mara S. M. Orescanin

B.A., Carleton College (2006)

M.S., University of Illinois at Urbana Champaign (2009)

Submitted to the Joint Program in Applied Ocean Science & Engineering

in partial fulfillment of the requirements for the degree of

Doctor of Philosophy

at the

MASSACHUSETTS INSTITUTE OF TECHNOLOGY

and the

WOODS HOLE OCEANOGRAPHIC INSTITUTION

September 2015

Author . . . . . . . . . . . . . . . . . . . . . . . . . . . . . . . . . . . . . . . . . . . . . . . . . . . . . . . . . . . . . . . . . . . . . . .

Joint Program in Oceanography/Applied Ocean Science & Engineering

Massachusetts Institute of Technology

& Woods Hole Oceanographic Institution

August 19, 2015

Certified by . . . . . . . . . . . . . . . . . . . . . . . . . . . . . . . . . . . . . . . . . . . . . . . . . . . . . . . . . . . . . . . . . . . . .

Steve Elgar

Senior Scientist, Applied Ocean Physics and Engineering

Woods Hole Oceanographic Institution

Thesis Supervisor

Accepted by . . . . . . . . . . . . . . . . . . . . . . . . . . . . . . . . . . . . . . . . . . . . . . . . . . . . . . . . . . . . . . . . . . . .

David E. Hardt

Chairman, Committee for Graduate Students

Massachusetts Institute of Technology

Accepted by . . . . . . . . . . . . . . . . . . . . . . . . . . . . . . . . . . . . . . . . . . . . . . . . . . . . . . . . . . . . . . . . . . . .

Henrik Schmidt

Chairman, Joint Committee for Applied Ocean Science & Engineering

Massachusetts Institute of Technology

Woods Hole Oceanographic Institution

# Hydrodynamics of a Multiple Tidal Inlet System:

# Katama Bay, Martha's Vineyard, MA

by

Mara S. M. Orescanin

## Abstract

Observations, theoretical models, and a numerical model (ADCIRC) are used to investigate the effects of tides, waves, bay bathymetry, and changing inlet geometry on the hydrodynamics of the multiple-inlet Katama system, Martha's Vineyard, MA. Momentum fluxes from breaking waves drive water into the inlet, nearly stopping the 2 m/s ebb currents during a hurricane. The evolving morphology of Katama Inlet has a dominant effect on tidal distortion and bay circulation. As Katama inlet lengthened, narrowed, and shoaled between 2011 and 2014, the relative effects of friction (observed and simulated) increased greatly, resulting in reduced circulation energy, an increase in the M6 tidal constituent, and changes in velocity asymmetries that are consistent with an evolution from flood to ebb dominance. The effects of changing inlet parameters (e.g., inlet geometry, bay bathymetry, friction, tidal forcing) are quantified via a lumped element model that accounts for the presence of a shallow flood shoal that limits flow from the ocean into the bay. As the difference in depth between inlet and flood shoal increases, the amplitude and phase of the incoming tide are increasingly modified from predictions without a flood shoal, and flows into the bay are further hindered.

# Dedication

To Marko, my love, and to our darling minions, Maksim and Olivia Zoni: you are the light of my life

*"Behind all seen things lies something vaster; everything is but a path, a portal or a window opening on something other than iteself." -Antoine de St. Exupery, Wind, Sand, and Stars*

# Biography

Mara's first memory is of visiting the beaches of Monterey Bay, CA, looking for seashells, examining the kelp and driftwood, and eating sand. Her passion for the natural world, and in particular the ocean, grew and inspired her to study physics at Carleton College. A study abroad trip to Sri Lanka introduced Mara to geology, which ultimately lead her to earn double Master's degrees in Geology and Theoretical and Applied Mechanics at the University of Illinois, Urbana Champaign. A trip to visit the beaches of Puerto Rico inspired Mara to apply to the Joint Program in Oceanography to study coastal processes, where she began in Fall 2010.

Mara met her husband, Marko, while both were studying at the University of Illinois. Together they have two children, Maksim, born during the end of Mara's Master's degrees, and Olivia, born just before Mara completed her qualifying exam at MIT.

# Acknowledgments

This dissertation could not have been completed without the support of my advisor Steve, and co-advisor Britt. I am eternally grateful to you both for taking a chance on a me. I truly have enjoyed all I've learned from you while pursuing this degree, and it has not felt like five years have passed. Thank you for providing the environment and support for me to learn to be an independent researcher and for challenging me to grow. Thanks also for telling and re-telling the countless hilarious stories of days passed.

Thanks to my committee members, Pierre Lermusiaux and Tony Dalrymple. I have enjoyed your mentorship, guidance, and patience over the course of my research. Having a fresh perspective on this work has been invaluable.

Thanks to Maria Brown, David Clark, Danik Forsman, Levi Gorrell, Jeff Hansen, Sean Kilgallin, Melissa Moulton, Christen Rivera-Erick, Jenna Walker, Anna Wargula, Regina Yopak, and Seth Zippel for helping to obtain the data, Maddie Smith for drag coefficients based on vertical velocities, Janet Fredericks for help with the MVCO data, Clare Gesualdo, Charlie Blair, and the Edgartown Reading Room for providing pier pilings for pressure gages and moorings for small boats, and Mike Creato for providing staging space and a pleasant place to work at Katama Airpark. Thanks to Jason Flemming for help during the ADCIRC Boot Camp, and Julia Hopkins for help with bathymetry for model grids.

Infinite thanks goes to my family for their loving support. To Marko, you are my lighthouse and I would not have had the strength to undertake these past five years without your constant love. To Maksim and Olivia Zoni, thank you for being the best children I could ask for, and for understanding that sometimes Mama has to "visit her advisor". Thank you for your developing patience! I love watching you grow and nurture your curiosity and can't wait to continue this journey with you. To my mother, father, and sister: Thank you for providing the foundation for my own curiosity and for the countless trips to the beach! I never doubted I was capable of anything thanks to your loving support. Thanks to my cousin, Tina, who knows all to well the bumps in this road. Thanks to the countless friends, who helped me laugh through all the hard times.

# Contents

# List of Figures

14

# List of Tables

# Chapter 1

# Introduction

Tidal inlets are ubiquitous global features that connect back bays and estuaries to the ocean (Haupt (1889); Keulegan (1967); Nichols and Marson (1939); Stanev et al. (2003), and many others). In many cases, bays are connected to the ocean via several inlets (Kraus and Militello (1999); Pacheco et al. (2010); Salles et al. (2005), and many others), although usually the oceanic tidal forcing is the same at each inlet. Here, the hydrodynamics of the multiple-inlet Katama system on Martha's Vineyard, MA are investigated. Unlike bays with multiple inlets with similar tidal forcing, the two inlets connecting to Katama Bay have different tidal amplitudes and phases.

The organization of the dissertation is as follows. This chapter gives an overview to the history of the field site and its morphologic evolution. The subsequent chapters are written to be stand-alone works and each contains an introductions. Chapter 2 was published in *Continental Shelf Research* and quantifies the effects of wave forcing on one inlet with observations and a one-dimensional physical model (`http://www.sciencedirect.com/science/article/pii/S0278434314001356`). In Chapter 3 the changes in circulation observed over three years as the geometry and orientation of Katama Inlet evolved is examined. The observations are combined with numerical model (ADCIRC) simulations to investigate the effect of changing geometry and friction. Chapter 3 has been submitted to *Continental Shelf Research.* The effect of inlet location, geometry, and the effect of bay bathymetry on circulation is studied with a lumped element model for inlet impedance in Chapter 4. A summary of the results and suggestions for future research are presented in Chapter 5.

## 1.1   Location and Historical Background

The field site is Katama Bay, Martha's Vineyard, MA (Figure 1-1), home to one of New England's premier harbors (Edgartown, MA), as well as significant shellfishing. Katama Bay is a small ($\sim$7 km$^2$), shallow ($<$3 m), well-mixed bay that is connected to Vineyard Sound to the north by Edgartown Channel, and to the Atlantic Ocean to the south by Katama Inlet. Katama Inlet is ephemeral, and has an approximate 10-15 cycle of breaching near the center of the sand barrier (Norton Point) separating the bay from the ocean (Figures 1-1 and 1-2), migrating eastward more than 2 km, and eventually closing along the eastern most part of Katama Bay along Chappaquiddick Island [Ogden (1974)]. Waves from the Atlantic Ocean can enter Katama Inlet, although usually wave energy is reduced by breaking on the ebb shoal offshore of the inlet mouth. The momentum from breaking waves can force water into the inlet (see Chapter 2 for analysis).

The inlet remained closed from the 1960's until it breached during the Patriots' Day storm in 2007 (Figure 1-2). Between 2007 and 2011, when the fieldwork for this study began, the inlet widened significantly (2008, Figure 2), and migrated approximately 2 km toward the east. In summer-fall 2011, pressure sensors, acoustic Doppler current profilers (ADCPs), and acoustic Doppler velocimeters (ADVs) were deployed to measure tidal levels, waves, and currents within the Katama system. The observations include waves and currents during Hurricanes Irene (August 2011) and Sandy (October 2012). In both cases, waves were greater than 10 m high in deep water on the continental shelf, and were about 5 m high in 12-m water depth just offshore of Katama Inlet (further description in Chapters 2 and 3).

In 2013, the Norton Point sand spit started to extend along the south coast of Chappaquiddick Island (Figure 1-3). Between summer 2013 and the summer 2014, the spit elongated over 500 m. The spit continued to grow, and extended nearly an additional km between June 2014 and April 2015, when it closed (Figure 1-3, April 2015).

From 2011 to 2015, the inlet evolved from a short (200 m), wide (450 m), deep (4.0 m) opening oriented roughly north-south (Figure 1-2, 2011) to a long ($>$ 1 km), narrow (150 m), shallow (1.5 m) channel oriented nearly east-west (Figure 1-3). The evolving inlet resulted in a strong decrease in overall circulation energy that is simulated accurately by the ADCIRC numerical model (further addressed in Chapters 3 and 4).
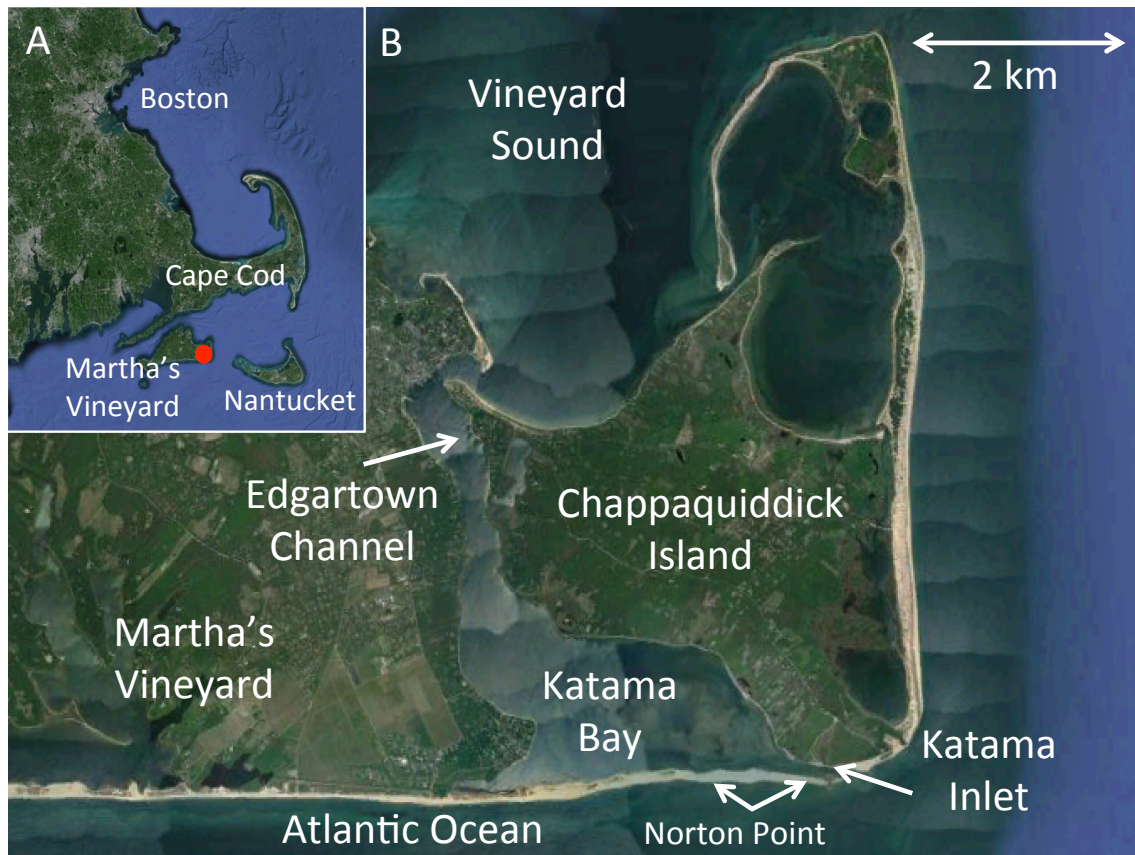
Figure 1-1: Map of A) Southeastern New England with Katama Bay on Martha's Vineyard indicated by the red circle, and B) close up of Katama Bay with Edgartown Channel to the north (up) and Katama Inlet to the south. When Katama Inlet is closed, Norton Point extends continuously from Martha's Vineyard to Chappaquiddick Island.
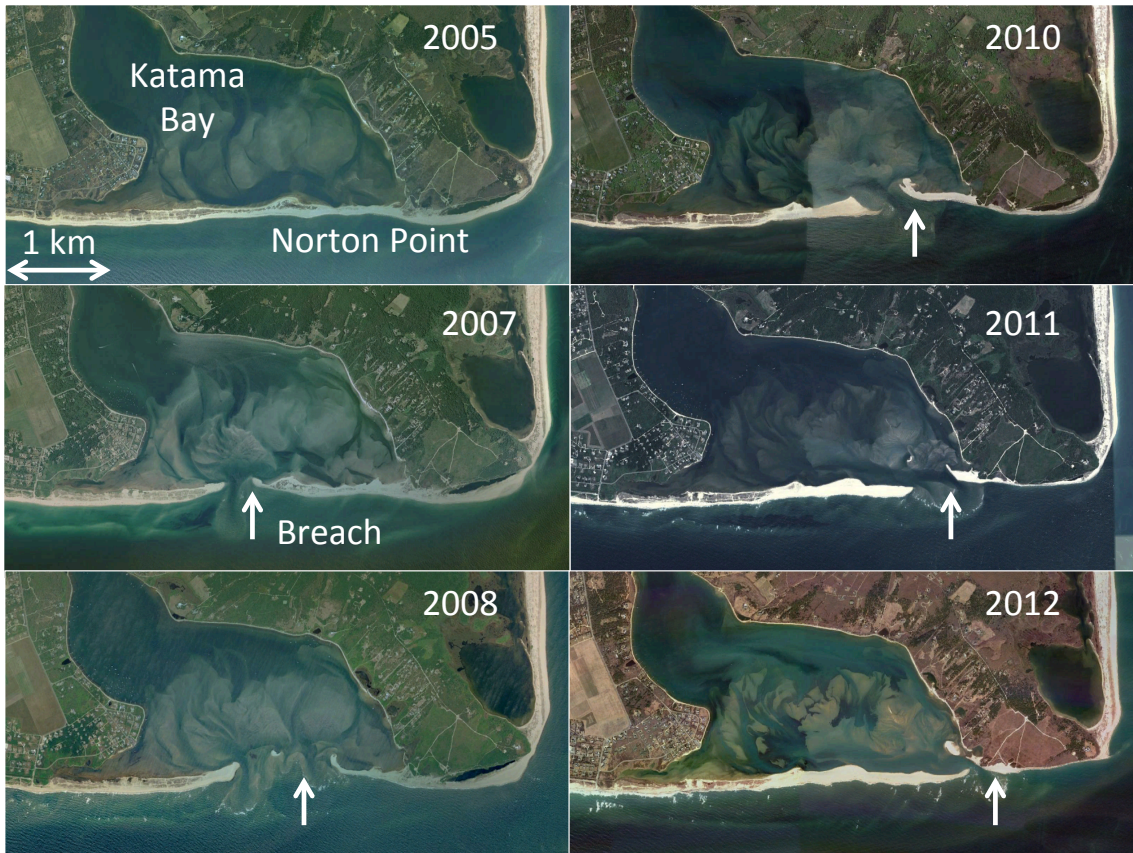
Figure 1-2: Katama Inlet breach eastward migration 2005-2012. Initial breach occurred April 2007 along the western side of Norton Point and has migrated rapidly to the eastern side of Katama Bay, as indicated by the white arrow in each frame. Images courtesy of Google Earth.
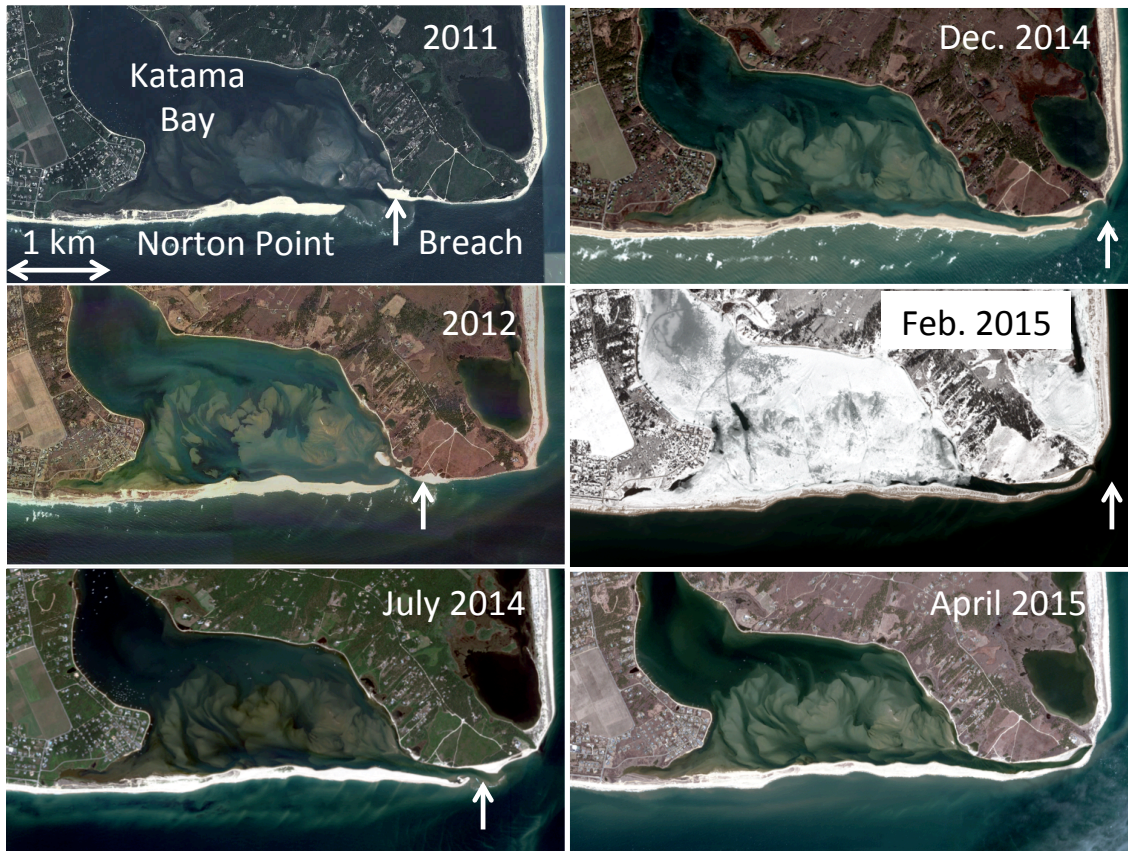
Figure 1-3: Recent evolution of Katama Inlet since study initiated in summer 2011. The wrapping of the inlet around the southern part of Chappaquiddick began in early 2013 (no image). Images in 2011 and 2012 courtesy of Google Earth. Images 2014 and 2015 taken from Pleiades satellite.

# Chapter 2

# Observations of wave effects on inlet circulation

*This chapter has been published in Continental Shelf Research with co-authors Britt Rauben-heimer and Steve Elgar and is included with permission (`http://www.sciencedirect.com/science/article/pii/S0278434314001356`).*

## 2.1  Abstract

Observations of water levels, winds, waves, and currents in Katama Bay, Edgartown Channel, and Katama Inlet on Martha's Vineyard, Massachusetts are used to test the hypothesis that wave forcing is important to circulation in inlet channels of two-inlet systems and to water levels in the bay between the inlets. Katama Bay is connected to the Atlantic Ocean via Katama Inlet and to Vineyard Sound via Edgartown Channel. A numerical model based on the momentum and continuity equations that uses measured bathymetry and is driven with observed water levels in the ocean and sound, ocean waves, and local winds predicts the currents observed in Katama Inlet more accurately when wave forcing is included than when waves are ignored. During Hurricanes Irene and Sandy, when incident (12-m water depth) significant wave heights were greater than 5 m, breaking-wave cross-shore (along-inlet-channel) radiation stress gradients enhanced flows from the ocean into the bay during flood tides, and reduced (almost to zero during Irene) flows out of the bay during ebb tides. Model simulations without the effects of waves predict net discharge from the sound to the ocean both during Hurricane Irene and over a 1-month period with a range of conditions.

In contrast, simulations that include wave forcing predict net discharge from the ocean to the sound, consistent with the observations.

## 2.2   Introduction

Inlets are common coastal features connecting bays and estuaries with the open ocean. Flows through inlets can transport sediments, pollutants, nutrients, and other materials both into and out of the bay, affecting navigation, swimmer safety, and water quality. Although flows in inlets often are driven by tides, the effects of ocean surface gravity waves on the circulation, morphology, and stability of inlet channels have been hypothesized for decades [Bruun (1978); LeConte (1905); O'Brien (1931, 1969); Stevenson (1886)]. Recently the importance of ocean surface waves to inlet dynamics has been investigated with numerical models [Bertin et al. (2009); Dodet et al. (2013); Malhadas et al. (2009); Olabarrieta et al. (2011)].

As wind-generated surface waves (swell and sea) break in the shallow water depths on the ebb shoals offshore of inlet mouths and on the beaches alongshore of the inlet, their momentum is transferred to the water column. Gradients in wave radiation stresses caused by wave breaking can raise water levels (setup) near the shoreline [Longuet-Higgins and Stewart (1964)], and drive alongshore currents if incident waves propagate at an angle to the shoreline [Longuet-Higgins (1970)]. Unlike an ocean beach, there is no physical barrier at an inlet mouth, and thus wave radiation stress gradients have been hypothesized to drive flow into the inlet channel, raising water levels in the bay [Bertin et al. (2009); Dodet et al. (2013); Malhadas et al. (2009); Olabarrieta et al. (2011)]. Similarly, wave-induced setup along the shoreline to the sides of inlet channels can produce areas of relatively high water level compared with the level in the channel, also driving water toward the inlet mouth [Apotsos et al. (2008); Malhadas et al. (2009)].

Although theory and numerical models [Bertin et al. (2009); Dodet et al. (2013); Malhadas et al. (2009); Olabarrieta et al. (2011)] suggest waves can affect water levels and currents near and within inlets, there are few observational tests of these hypotheses. Recent numerical results [Bertin et al. (2009); Dodet et al. (2013); Malhadas et al. (2009); Olabarrieta et al. (2011)] show an increase in bay water levels and changes to inlet flows resulting from surface gravity waves.

There have been many studies of bays with two or more inlets, but most have considered systems with the same tidal forcing at all the inlets and have focused on morphological stability [Aubrey and Giese (1993); Bruun and Adams (1988); Salles et al. (2005); van de Kreeke et al. (2008)]. Straits forced by different tides on either end also have been investigated [Campbell et al. (1998); Easton et al. (2012); Stevens et al. (2008)], but wave effects were not included.

Here, observations of water levels, winds, waves, and currents in Katama Inlet and Bay, MA (Figure 2-1), including those during Hurricanes Irene and Sandy, combined with a numerical implementation of the momentum and continuity equations [Malhadas et al. (2009)] extended to account for different tidal forcing at either end of Katama Bay are shown to be consistent with the hypothesis that wave radiation stresses result in increased flow into the inlet.

## 2.3 Theory and model

Simplifying the governing equations to a first-order approximation, the hydrodynamics of the Katama Bay system, including Edgartown Channel and Katama Inlet, are described by the cross-shore momentum balance and continuity (mass conservation). Nonlinear-advective terms, to a first order approximation, are assumed to cancel [Jay (1991); Olabarrieta et al. (2011)] or to be small [Lentz et al. (1999)]. Given the small spatial scales, Coriolis terms are small. Therefore, the depth-averaged, cross-shore (along-inlet) momentum balance for each inlet is [Campbell et al. (1998); Malhadas et al. (2009); Proudman (1953)]:

$$\frac{\partial Q}{\partial t} = \triangledown P - C_d b \frac{|Q|Q}{A^2} + R_s b + \frac{\rho_a}{\rho_\omega} \tau_\omega b \tag{2.1}$$

where $Q$ is the volume discharge given by the velocity, $v$, in the inlet times the cross-sectional area, $A$, $t$ is time, $\triangledown P$ is a pressure gradient, $C_d$ is the bottom friction coefficient, $R_s$ is the radiation stress gradient in the cross-shore direction, $b$ is the width of the inlet, $\rho_a$ and $\rho_w$ are the densities of air and water, respectively, and $\tau_w$ is the wind stress. The pressure gradient is given by:

$$\triangledown P = g \frac{\eta_0 - \eta_B}{L} A \tag{2.2}$$

29
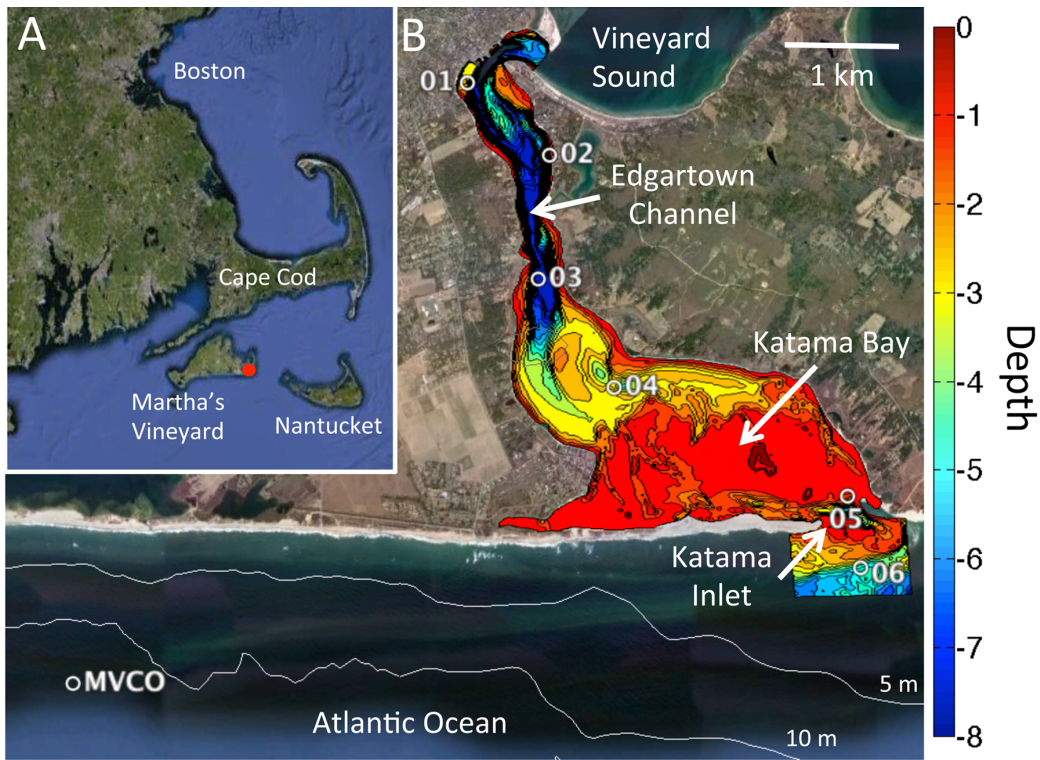
Figure 2-1: Map of site location: (A) Google Earth image of eastern Massachusetts, Cape Cod, Nantucket, and Martha's Vineyard. The red circle indicates the location of Katama Bay. (B) Katama Bay, located on the eastern edge of Martha's Vineyard, and the surrounding nearshore region offshore of Katama Inlet. Water depth is indicated by the color contours (scale on the right) and contour curves (labeled with depth). Symbols indicate pressure sensors (01, 02), colocated pressure and current sensors (04, 05, 06), and colocated pressure sensors and current profilers (03, MVCO). The Martha's Vineyard Coastal Observatory (MVCO) observations were obtained in 12-m water depth.

where $g$ is the gravitational constant, $\eta_0$ is the sea level in the sound or ocean and $\eta_B$ is the sea level of the bay, and $L$ is the inlet length. The bottom stress is estimated from a quadratic drag relationship, with the bottom friction coefficient estimated from observations (discussed below). The wave forcing in the ocean is given by the gradient in radiation stress, calculated as [Apotsos et al. (2008)]:

$$R_s = \frac{1}{16}gH_b^2 \left( \frac{\cos^2(\theta) + 0.5}{\triangle x} \right) \tag{2.3}$$

where $H_b$ is the significant wave height (four times the standard deviation of sea-surface fluctuations between 0.05 and 0.30 Hz) at breaking, $\theta$ is the wave direction relative to the inlet channel axis, and $\triangle x$ is the distance from the location of wave breaking to the inlet mouth. Wave radiation stress is assumed negligible in Vineyard Sound, and thus is neglected in the momentum equation for Edgartown Channel.

The wind stress, $\tau_\omega$ is calculated by Large and Pond (1981) [Large and Pond (1981)]:

$$\tau_\omega = C_{d\omega}|u_{10}|u_{10} \tag{2.4}$$

where $C_{d\omega}$ is the drag coefficient for wind over water and $u_{10}$ is the along-inlet component of the wind velocity at 10 m above the water-air interface. Winds are assumed uniform over the model domain.

For the case considered here where there are two inlets (Figure 2-2), each with different tidal forcing and geometry, momentum equations must be solved for the flow in both inlets. Conservation of mass (continuity) implies:

$$\frac{\partial \eta_B}{\partial t} = \frac{Q_1 + Q_2}{A_B} \tag{2.5}$$

where the subscripts 1 and 2 refer to the discharge from each of the two inlets and $A_B$ is the surface area of the bay. Thus, the two momentum Equations 2.1 are coupled to each other via the continuity Equation 2.5.

Momentum balances and continuity are applied simultaneously at Katama Inlet and Edgartown Channel. The model is driven with sea level fluctuations owing to tides, storm surge, and other large scale processes observed in the ocean (MVCO, Figure 2-1) and sound (sensor 01, Figs. 2-1 and 2-2), waves observed in 12 m depth offshore of Katama Inlet

31
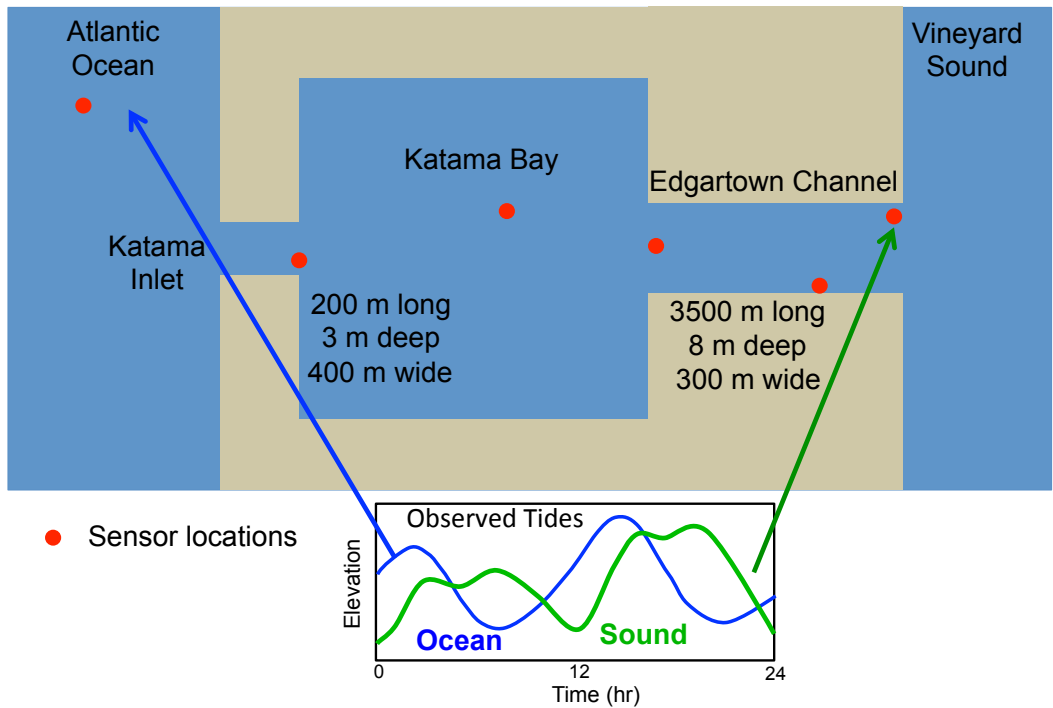
Figure 2-2: Schematic of the model domain. The inlet and bay dimensions were obtained from bathymetric surveys with GPS and sonar on a wave runner and on a small boat. The model is driven with sea level observed in the sound (01) and in the ocean (MVCO, 12-m depth, Figure 2-1), waves observed at MVCO, and winds observed near the shore onshore of MVCO. The model outputs are sea level in the bay (05) and velocities in Edgartown Channel (03) and Katama Inlet (05).

(MVCO, Figure 2-1), and winds observed near the shore onshore of MVCO. Ten-minute averages of observed quantities were interpolated to 1-minute values to drive the model, which was integrated in time using forward differences with 1-minute time steps. Estimates for bottom friction and inlet dimensions come from field data, described in Section 2.4. Model output includes water levels in the bay and velocities through each inlet channel, which are averaged over 10 minutes to match the 10-minute averages used for the observations.

## 2.4 Observations and data collection

### 2.4.1 Location description

Katama Bay is located on Martha's Vineyard, an island south of Cape Cod (Figure 2-1A). Martha's Vineyard and Nantucket Islands form a barrier between the open Atlantic Ocean to the south and east and Vineyard Sound to the north (Figure 2-1A), resulting in spatially complex tidal patterns [Chen et al. (2011); Shearman and Lentz (2004)]. The bay has a surface area of approximately 7.5 x 106 m$^2$, and water depths range from 10 m at the north end where it connects to Edgartown Channel (sensor 03, Figure 2-1) to less than 1 m in the southern half (red contours in Figure 2-1). There is no major source of fresh water, and the waters are well mixed, with salinity about 32 PSU throughout the system.

Katama Bay is located on Martha's Vineyard, an island south of Cape Cod (Figure 2-1A). Martha's Vineyard and Nantucket Islands form a barrier between the open Atlantic Ocean to the south and east and Vineyard Sound to the north (Figure 2-1A), resulting in spatially complex tidal patterns [Chen et al. (2011); Shearman and Lentz (2004)]. The bay has a surface area of approximately 7.5 x 106 m$^2$, and water depths range from 10 m at the north end where it connects to Edgartown Channel (sensor 03, Figure 2-1) to less than 1 m in the southern half (red contours in Figure 2-1). There is no major source of fresh water, and the waters are well mixed, with salinity about 32 PSU throughout the system.

### 2.4.2 Measurements

**Surveys and inlet dimensions**

The bay, inlet channels, and ebb shoal were surveyed with GPS and sonar mounted on a wave runner (Figure 2-1). In addition, detailed cross-sections of the inlet channels were

obtained with GPS and sonar mounted on a small boat (Figure 2-3). The channel geometries were approximated with triangles that preserve the cross-sectional area (Figure 2-3). The surveys and approximations provide the dimensions of the inlets (L, A, b) and bay (AB) used in the model. Katama Inlet is 2 to 6 m deep, approximately 300 m long, and 400 m wide (Figure 2-3B), whereas Edgartown Channel is 2 to 10 m deep, approximately 2500 m long, and 350 m wide (Figure 2-3A). The widths and depths of the channels (and the triangular approximations, Figure 2-3) depend on the sea level within the channel, which is estimated as the average depth between the bay and the ocean (Katama Inlet) or the sound (Edgartown Channel).

**Hydrodynamic observations**

Observations were obtained between mid August and early October 2011 at locations 01, 02, 03, 04, and 05, from mid September until early October at 06, and again for several days during the passage of Hurricane Sandy in late October 2012 at locations 01 and 05 (see Figure 2-1 for locations). Pressure gages were mounted near the seafloor at all sensor locations, and were colocated with an acoustic Doppler current profiler (ADCP) in 10 m depth where Edgartown Channel meets the bay (03), and with acoustic Doppler velocimeters (ADV) in Katama Inlet (05) and on the outer edge of the ebb shoal in approximately 5 m depth (06). The pressure gages and ADVs were sampled at 2 Hz, and the ADCP samples were 1-minute averages. Bottom pressures were corrected for atmospheric pressure fluctuations and converted to sea-surface elevation fluctuations assuming hydrostatic pressure and using linear theory. The ADV sample volumes were approximately 0.8 m above the sandy bottom. The flows at sensor 05, which is on the northern end of Katama Inlet, are assumed to represent the inlet currents, and the water levels at sensor 05 are used as a proxy for the bay water levels. In addition, water levels, significant wave heights, wave spectra, and wave directions were obtained in 12-m water depth (MVCO, Figure 2-1), and wind was measured near the shoreline onshore of the 12-m depth sensors.

**Waves**

Incident (12-m water depth) significant wave heights ranged from 0.3 to 5.5 m (Figure 2-4A), peak periods from 5 to 12 seconds, and mean wave directions from 160 to 210 degrees (close to normally incident on the south facing beaches surrounding the mouth of Katama
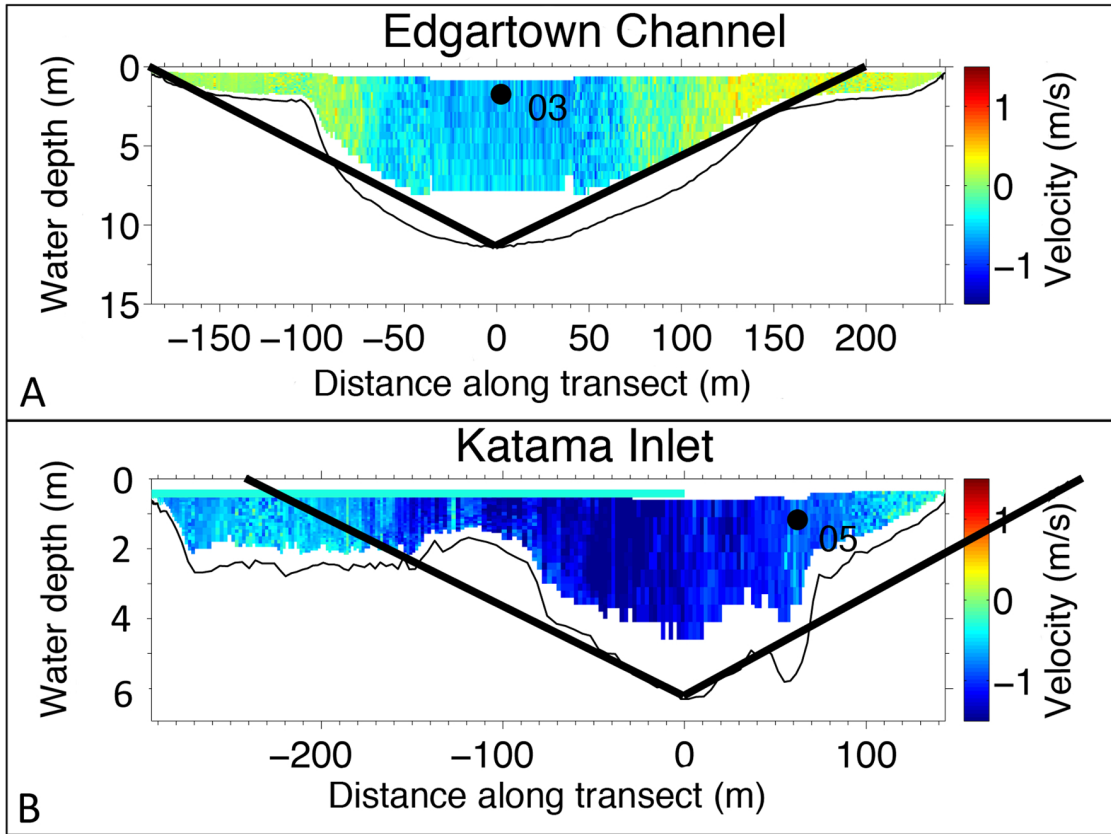
Figure 2-3: Water depth (thin black curves) and velocity (color contours, scale on the right) along the (A) Edgartown and (B) Katama inlet channel axes versus along-channel distance from the center of the channel. Thick black triangles are the approximations to the bathymetry used to estimate channel cross-sectional areas in the model. Positive velocity is northward flow (into the page) and negative velocity is southward flow (out of page). The currents were measured with an acoustic Doppler profiler mounted on a small boat with GPS that traversed the channels slowly (approximately 1 m/s). Simultaneous depth soundings were obtained with a vertical sonar beam. The black circles are the horizontal locations of the sensors in Edgartown Channel (03) and Katama Inlet (05).

Inlet). Waves in Vineyard Sound and especially in Edgartown Harbor were small, and are neglected here. Winds ranged from 0 to 17 m/s (Figure 2-4B).

Waves measured in 12 m depth (MVCO, Figure 2-1) were shoaled over the measured bathymetry (Figure 2-11) to the depth at breaking assuming that linear energy flux $EC_g$ is conserved, where $E$ is the wave energy and $C_g$ is the group velocity. Waves are estimated to begin to break when $\gamma = H_b \: / \: h = 0.8$, where h is the water depth. Different values of $\gamma$ do not affect the results significantly. Comparison with waves measured in 5-m water depth on the ebb shoal (sensor 06 in Figure 2-1) for the latter part of the 2011 observational period suggest shoaling the waves measured in 12-m depth to breaking is a reasonable approximation, and produces estimates of radiation stress gradients similar to those using the 5 m depth observations. Model results using the shoaled MVCO waves are not significantly different than those using the waves observed on the ebb shoal (06).
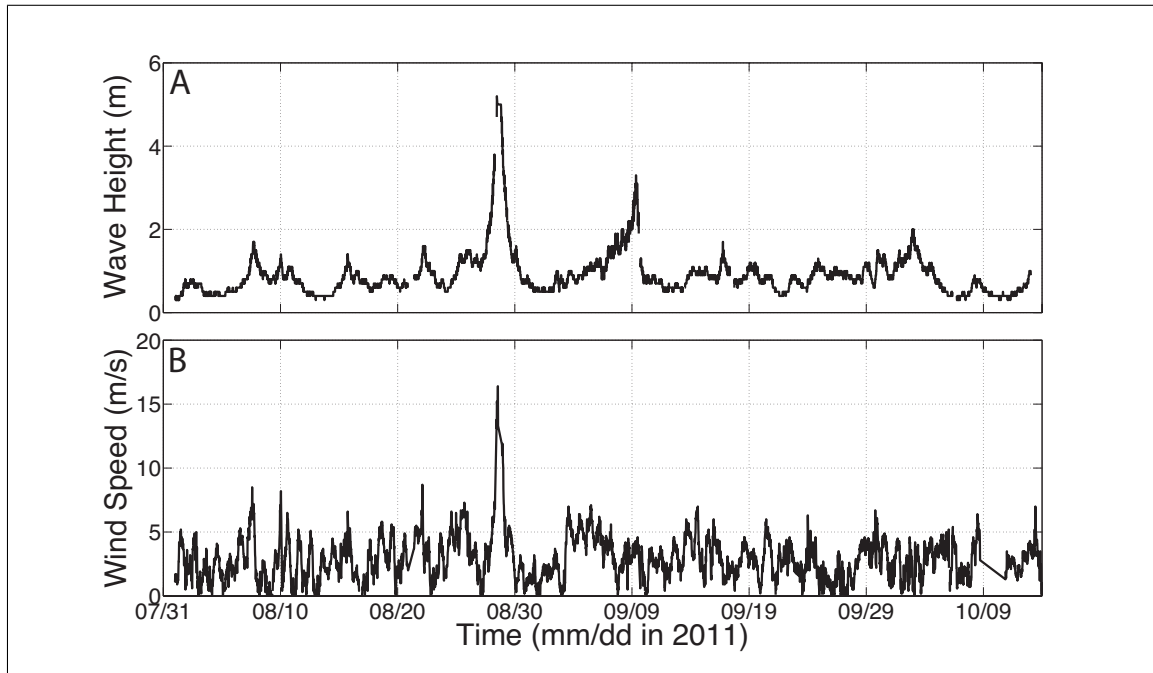


Figure 2-4: Field conditions: (A) Significant wave height (0.05 to 0.30 Hz) and (B) wind speed versus time. Waves were measured in 12-m water depth (MVCO, Figure 2-1), and winds were measured near the shoreline onshore of MVCO.

### 2.4.3 Bottom friction

The seafloor in Katama Inlet is sandy, with large (up to 1-m high and 10-m long) migrating bedforms reported by SCUBA divers, whereas the bottom in Edgartown Channel is smoother, and consists of harder, relatively immobile compacted finer sediments. Thus, the bottom friction coefficients of the two inlet channels may differ, and were estimated independently. Specifically, assuming a quadratic drag law, bottom friction coefficients, $C_d$, were estimated as the slope of a linear fit to pressure gradient versus $v|v|$ [Brown and Trask (1980); Campbell et al. (1998); Giese and Jay (1989); Kim et al. (2000)], where the pressure gradients were between sensors 02 and 04 (Edgartown Channel, Figure 2-1) and between sensors 04 and 06 (Katama Inlet, Figure 2-1), with velocity, $v$, measured between the pressure sensors at locations 03 (Edgartown Channel) and 05 (Katama Inlet). The fits were obtained when waves were small. The drag coefficients were $C_d$=0.007 at Edgartown and $C_d$=0.011 at Katama. These estimates are similar to those obtained from the profiling current meter assuming a logarithmic boundary layer for the relatively few cases with a good fit [Kim et al. (2000)], and to estimates based on the variance of the vertical velocities at sensor 05 [Elgar and Raubenheimer (2010); Nezu and Rodi (1986)].

## 2.5 Model-data comparisons

Tidal sea-level fluctuations observed in the ocean are larger than, and several hours out of phase with those observed in the sound [Chen et al. (2011); Shearman and Lentz (2004)]. Bay water levels observed near Katama Inlet (at 05) are between the ocean and sound water levels (Figure 2-5A). For mild wave conditions, the model predicts accurately the observed bay water levels (Figure 2-5B) whether or not wave forcing is included. During Hurricane Irene (Aug 28) incident significant wave heights were greater than 5 m, and the model predictions of bay water levels are more accurate when wave forcing is included (Figure 2-5B). Unlike previous numerical results [Dodet et al. (2013); Olabarrieta et al. (2011)], the increase in the bay water level owing to wave forcing is relatively small, as discussed below, likely because water flows out of the bay into Vineyard Sound through Edgartown Channel rather than accumulating in a closed basin.

In contrast to the bay water levels, wave forcing has a significant effect on the flows through Katama Inlet. Before (Aug 26 - 27) and after (Aug 29 - 30) the passage of Hurricane
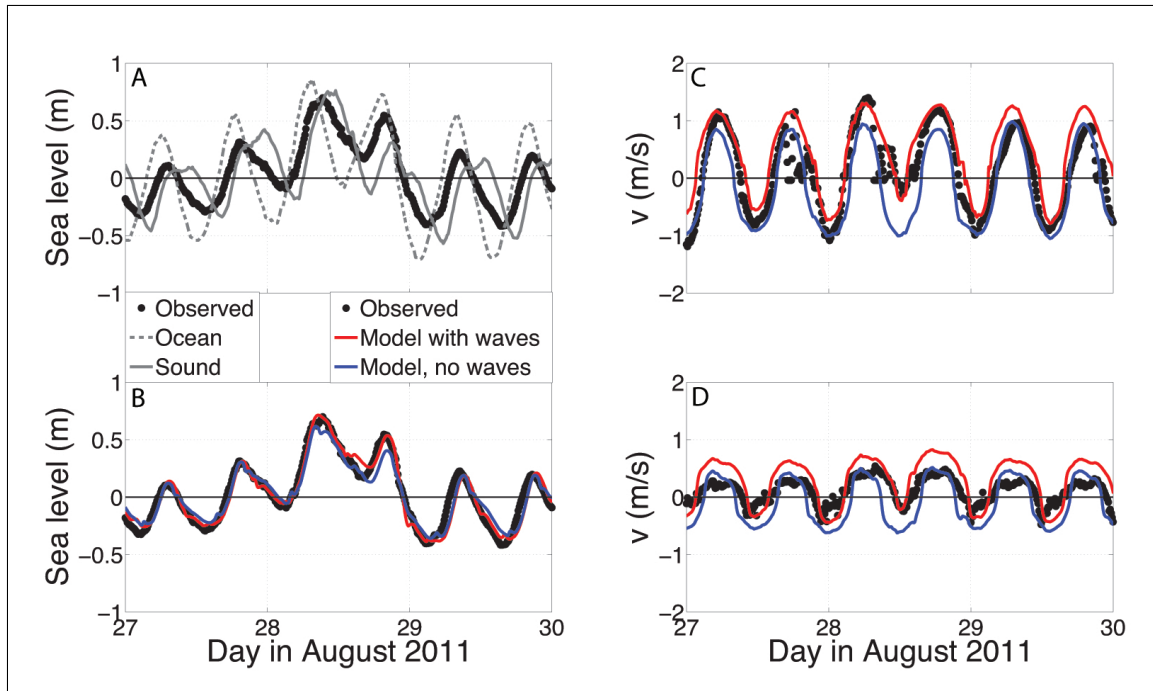
Figure 2-5: Model-data comparison for Hurricane Irene: (A) Sea level observed in the Atlantic Ocean (dashed grey curve), Vineyard Sound (grey curve), and in the bay near Katama Inlet (black dots, sensor 05 in Figure 2-1), and observed (black) and modeled (blue is model without waves, red is model with waves) (B) bay sea level near Katama Inlet (05), (C) velocity in Katama Inlet (05), and (D) velocity in Edgartown Channel (03) versus time. Positive velocity is northward flow (i.e., from the ocean to the bay and from the bay to the sound). Hurricane Irene was Aug 28, 2011.

Irene (Aug 28) waves were moderate (Figure 2-4), and both the model with and the model without waves predict the observed currents (Figure 2-5C). However, during Hurricane Irene (Aug 28), wave forcing resulted in enhanced flood flows and reduced (almost to zero) ebb flows, which is predicted by the model with waves, but not by the model without waves (Figure 2-5C). Simultaneously, during the hurricane the reduction in southward currents from the sound to the bay through Edgartown Channel is modeled more accurately if wave forcing is included than if waves are neglected (Figure 2-5D). Ten days after the passage of Hurricane Irene, an offshore nor'easter storm produced waves greater than 3 m (September 9, Figure 2-5A), resulting in enhanced flows into Katama Inlet that are predicted well by the model with wave forcing (not shown).

Although both Hurricane Irene and Hurricane Sandy had similar maximum wave heights ( 5 m in 12-m water depth), the biggest waves of Hurricane Irene occurred during low tide in the ocean (ebb flows in Katama Inlet, negative current speed, mid-day of Aug 28, Figure 2-5C) and the biggest waves of Hurricane Sandy occurred during high tide in the ocean (mid-day of Oct 29, Figure 2-6C). Similar to Irene, model simulations suggest that waves force ocean water into the bay during Sandy (Figure 2-6C, compare red with blue curves). Strong easterly winds during Sandy produced elevated water levels at tide stations throughout Vineyard Sound (not shown), with some of the highest levels observed in Edgartown Channel, resulting in an extended period of high water levels during the storm (Figure 2-6A), and a corresponding decrease in the flood flow at Katama Inlet (Figure 2-6C). Without considering the effect of waves, the model predicts an ebb flow at Katama Inlet during the peak of Hurricane Sandy instead of the observed flood flow (Figure 2-6C, late on Oct 29). The model with waves predicts the weak flood flows, similar to the observations at the inlet. This change in sign could have significant impacts on sediment transport and discharge.

During the observational period there were several events with significant wave heights greater than about 2 m (Figure 2-4A and Hurricane Sandy). As wave heights increase, the root mean square errors between observed currents in Katama Inlet and those predicted by the model without waves increase, whereas the root mean square errors in currents simulated by the model with wave forcing remain approximately constant (Figure 2-7). For energetic waves the errors in the model with wave forcing are about one-half as large as those for the model without wave forcing.

The model simulations and the observations are consistent with the hypothesis [Bertin
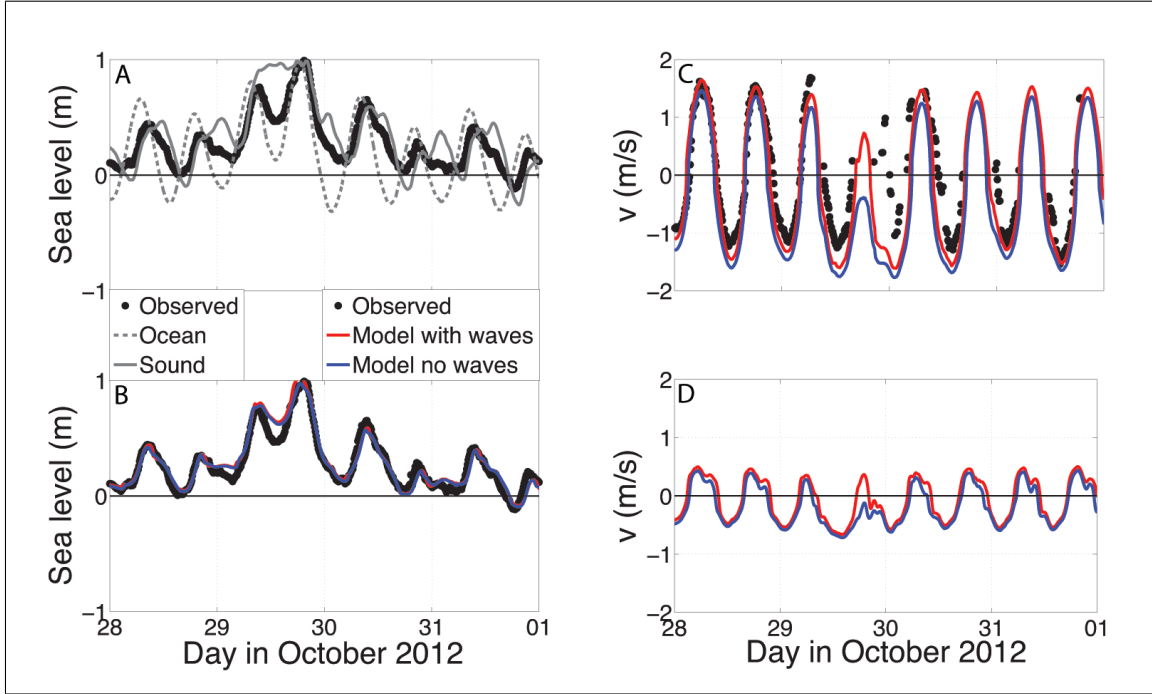
Figure 2-6: Model-data comparison for Hurricane Sandy: (A) Sea level observed in the Atlantic Ocean (dashed grey curve), Vineyard Sound (grey curve), and in the bay near Katama Inlet (black dots, sensor 05 in Figure 2-1), and observed (black) and modeled (blue is model without waves, red is model with waves) (B) bay sea level near Katama Inlet (05), (C) velocity in Katama Inlet (05), and (D) velocity in Edgartown Channel (03) versus time. Positive velocity is northward flow (i.e., from the ocean to the bay and from the bay to the sound). Hurricane Sandy was Oct 29, 2012.

et al. (2009); Dodet et al. (2013); Malhadas et al. (2009); Olabarrieta et al. (2011)] that wave forcing is important to circulation near an inlet. However, unlike previous numerical studies of inlets connecting enclosed basins with the ocean, in this two-inlet system wave radiation stresses resulted in only a small increase in bay water levels (Figs. 2-5 and 2-6). For a closed basin, the water forced into the inlet by wave radiation stresses produces increased bay water levels and a seaward pressure gradient. For Katama, the increased flow from the ocean into the bay can continue to flow northward through Edgartown Channel into Vineyard Sound (Figure 2-1). The observed net discharge from Aug 25 until Sep 25, 2011 was from the ocean through the bay to the sound, opposite to the net discharge predicted by the numerical model without wave forcing. In contrast, the net discharge predicted by the model with wave forcing was in the same direction as the observations, both during Hurricane Irene and over a 1-month period with a range of conditions (not shown).
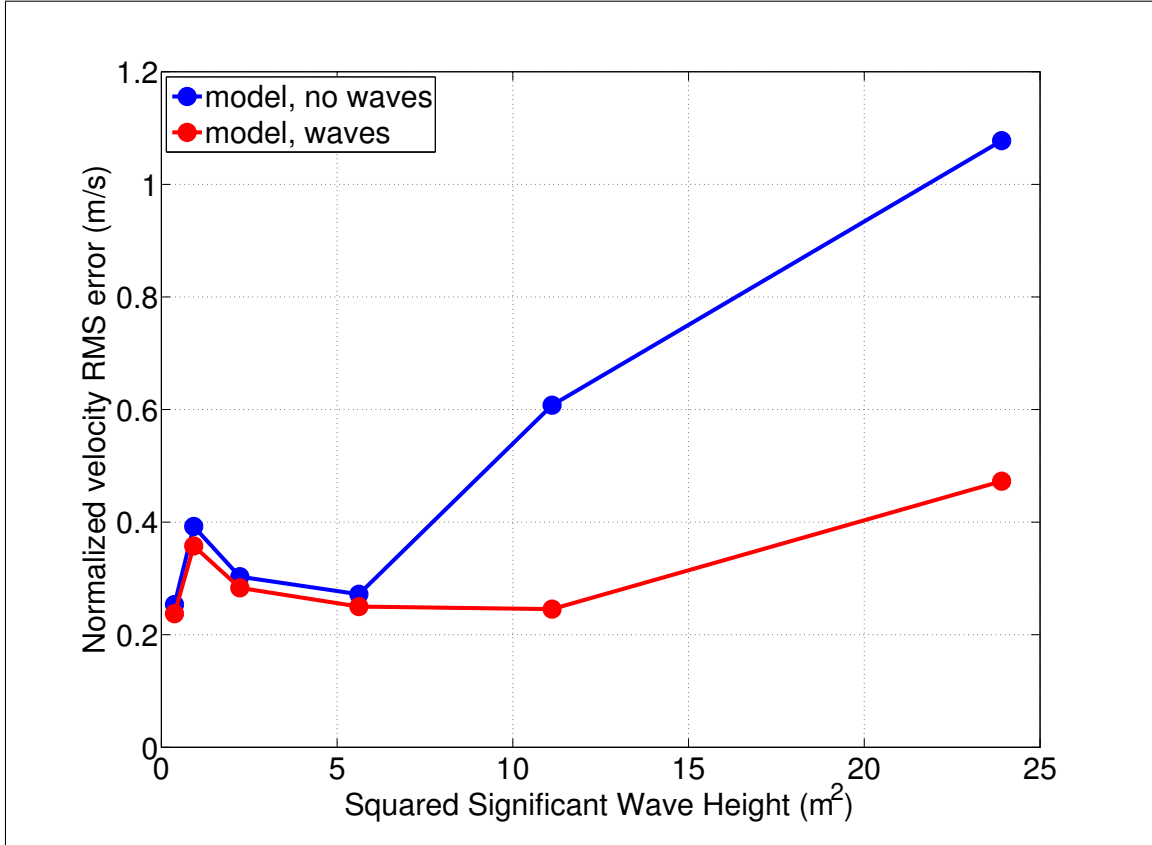
Figure 2-7: Root mean square (RMS) error between modeled and observed velocity normalized by the root mean square of the observed velocity in Katama Inlet versus squared offshore significant wave height (proportional to radiation stress) for the model with (red curve) and without (blue curve) wave forcing.

## 2.6 Model errors

The wind stress term was significantly smaller than the other terms in the momentum balance (Equation 2.1), even during hurricanes, either owing to the local wind speed or to the wind direction. Similarly, the temporal changes in discharge also were much smaller than the other terms in the momentum equation (Equation 2.1). Thus, the dominant terms in the momentum balance are the pressure gradients between the sound, ocean, and bay, wave radiation stresses acting on Katama Inlet, and bottom stress owing to friction of the flows in the inlet channels.

The numerical model assumes inlet flows are uniform both in the vertical and across the inlet channel. Transects across the channels with an acoustic Doppler profiling current meter are consistent with the assumption of little vertical shear (Figure 2-3), but indicate there is

41

some horizontal shear, especially between the center of Edgartown Channel and the shoals on its sides (Figure 2-3A). However, although possibly important to the three-dimensional circulation and to the discharge magnitude, the shear in Edgartown Channel does not affect the conclusion presented here based on the one-dimensional model that waves are important to the circulation.

The model depends on the geometry of the inlets and the bay. The bay surface area was obtained from wave runner-based bathymetric surveys (Figure 2-1), which may not estimate the location of the shoreline accurately. Moreover, the cross-sections of the inlet channels are approximated as triangles (Figure 2-3). However, numerical experiments (not shown) suggest the results are not sensitive to different approximations to the channel cross-section, including the triangular approximation used here.

During Hurricanes Irene and Sandy and the nor'easter storms, waves may have been breaking offshore of the MVCO site (Figure 2-1), resulting in an underestimation of the radiation stress forcing, and thus an underestimation of the effects of wave forcing (e.g., the red curves in Figure 2-5 during Hurricane Irene, Aug 28 and in Figure 2-6 during Hurricane Sandy, Oct 29).

Although the one-dimensional model used here is sufficient to address the hypothesis [Bertin et al. (2009); Dodet et al. (2013); Malhadas et al. (2009); Olabarrieta et al. (2011)] that wave forcing is important to inlet currents (Figs. 2-5 and 2-6), a more sophisticated model [Hench and Luettich (2003); Olabarrieta et al. (2011); Wheless and Valle-Levinson (1996)] might produce more detailed results. For example, the model used here assumes that the water level in the bay responds uniformly to the forcing at the two inlets, and that the measurements at location 05 represent the bay water levels. However, there were variations in the water levels observed along the bay between Katama Inlet and Edgartown Channel. Similarly, for the frictionally dominated shallow inlets and bay considered here, nonlinear advective acceleration terms are assumed to be small, or to cancel [Jay (1991); Lentz et al. (1999); Olabarrieta et al. (2011)], but are included in other models. Although beyond the scope of this study, a more sophisticated modeling approach could resolve possible tilts in the bay water level, as well as two- and three-dimensional flow structures in the system.

## 2.7   Conclusions

Observations of water levels, winds, waves, and currents in Katama Bay and Inlet are consistent with the hypothesis [Bertin et al. (2009); Dodet et al. (2013); Malhadas et al. (2009); Olabarrieta et al. (2011)] that wave forcing is important to circulation in inlet channels and to water levels in the bay. A numerical model based on a balance of temporal changes in discharge, tidal- and surge-induced pressure gradients, and wave-radiation, wind, and bottom stresses, along with conservation of mass, predicts the currents observed in Katama Inlet more accurately when wave forcing is included than when waves are ignored. Including wave forcing reduces errors in model predictions of inlet current speeds to one-half the errors when waves are ignored.

During Hurricanes Irene and Sandy, wave radiation stresses caused enhanced flows into the bay during flood tides, and reduced (almost to zero during Irene) flows out of the bay during ebb tides. Unlike in closed basins, both the observed and modeled water levels in the bay did not increase greatly during storms, likely because water could flow from Katama Inlet through Edgartown Channel to Vineyard Sound. Consistent with observations, net discharge was from the ocean through the bay and out to the sound when waves are included in the model, but was in the opposite direction when waves were neglected. This wave-induced circulation pattern can lead to enhanced transport of sediments, nutrients, larvae, and other material into bays during storms, affecting navigation, water quality, shellfish farms, and possibly leading to closure of the inlet.

# Chapter 3

# Changes in Bay Circulation in an Evolving Multiple Inlet System

*This chapter has been submitted to Continental Shelf Research with co-authors Steve Elgar and Britt Raubenheimer*

## 3.1   Abstract

Observations and numerical model (ADCIRC) simulations are used to quantify the changes in circulation within the evolving, shallow, two-inlet tidal Katama system, Martha's Vineyard, MA. From 2011 to 2013, Katama Inlet, connecting Katama Bay to the Atlantic, became 5 times longer, 1/3 as wide, and 1/3 as deep as the inlet migrated and rotated. This morphological evolution caused a significant loss of energy throughout Katama Bay and Edgartown Channel, which connects the bay to Vineyard Sound. The decrease in energy between 2011 and 2013 was not monotonic. Model simulations suggest bathymetric changes caused by Hurricane Irene (August 2011) resulted in a temporary increase in circulation energy throughout the inlets and bay. Changes in the M4 and M6 tidal constituents, harmonics of the primary M2 tidal forcing, suggest the changes in the observed circulation patterns primarily were owing to changes in friction, and not to changes in advection resulting from the evolving inlet location, orientation, or geometry, consistent with previous results. Observed and modeled skewness and asymmetry of velocity fluctuations suggest that Katama Inlet evolved from flood to ebb dominance between 2011 and 2013, possibly contributing to its closure in 2015.

## 3.2 Introduction

Multiple tidal inlet systems are common coastal features that have complicated circulation patterns owing to the multiple connections between back bays and open water bodies. These coastal features are critical for ecological health, as well as for economic and recreational activities. Circulation in bays and estuaries depends on many factors, including the geometry of the inlets that connect these systems with the ocean (Aubrey and Speer (1985); Brouwer et al. (2013); Friedrichs et al. (1992); Speer and Aubrey (1985); Speer et al. (1991); van de Kreeke et al. (2008) and many others). Temporal changes in inlet geometry and the resulting changes to the circulation can affect navigability and the transport of nutrients throughout the system. In multiple-inlet systems, changes in the geometry of one inlet can affect the circulation differently than in systems with only one connection to the ocean [Brouwer et al. (2013); van de Kreeke et al. (2008)].

The effects of friction and advection are described by nonlinear terms in the equations of motion, and thus introduce overtides (harmonics of tidal constituents) and compound tides (combinations of lower-frequency tidal constituents) [Blanton et al. (2002); Parker (1991)]. Temporal changes in the inlet channel geometry can lead to changes in frictional and advective effects. Thus, changes in inlet geometry can alter the distortion of the nearly sinusoidal ocean tide [Aubrey and Speer (1985); Breaker et al. (2008); Dronkers (1986); Fortunato and Oliveira (2005); Friedrichs and Aubrey (1988); Friedrichs et al. (1992); Malhadas et al. (2009); Nidzieko (2010); Nidzieko and Ralston (2012); Speer and Aubrey (1985); Speer et al. (1991)]. Determining the relative influence of friction and advection as the inlet geometry evolves is important for understanding the mechanisms by which inlets close. Although theory and numerical models [Bertin et al. (2009); Dodet et al. (2013); Malhadas et al. (2009); Olabarrieta et al. (2011)] suggest waves can affect water levels and currents near and within inlets, there are few observational tests of these hypotheses. Recent numerical results [Bertin et al. (2009); Dodet et al. (2013); Malhadas et al. (2009); Olabarrieta et al. (2011)] show an increase in bay water levels and changes to inlet flows resulting from surface gravity waves.

Although tidal distortion and circulation in inlet systems have been studied for many years [Aubrey and Speer (1985); Dronkers (1986); Friedrichs et al. (1992); Geyer and Mac-Cready (2014); MacCready and Geyer (2010); Nidzieko (2010); Nidzieko and Ralston (2012); Prandle (1991); Speer and Aubrey (1985); Speer et al. (1991)], there are few field studies of

the effects of temporally changing inlet geometry in a multi-inlet system. Here, observations obtained over several years in the multi-inlet system of Katama Bay, Martha's Vineyard, MA (Fig. 3-1) are used to investigate the effects of the relatively rapidly changing Katama Inlet on the circulation and tidal distortion in the bay. Katama Bay is connected to Vineyard Sound through Edgartown Channel, and to the Atlantic Ocean through Katama Inlet (Fig. 3-1). Since 2011, Katama Inlet has migrated nearly 1500 m to the east, and its axis has rotated from a nearly N-S orientation to nearly E-W as the sand spit separating the bay from the ocean (Norton Point) has extended eastward and started to wrap around Chappaquiddick Island (Fig. 3-1B, C, D). Between 2011 and 2013, the length of Katama Inlet increased from 200 m to nearly 1000 m, the width decreased from 400 m to 150 m, and the depth decreased from 4.0 m to 1.5 m (Fig. 3-1C,D). Here, the observations are combined with 2D numerical model (ADCIRC) simulations to investigate the effects of the evolving inlet geometry on sea levels and currents within the Katama System, to determine the relative roles of friction and advection, and to quantify the tidal distortion.

## 3.3 Tidal distortion from friction and changing geometry

Inlets alter the properties of the ocean tide by acting as restrictions to flow from the coastal ocean to the back bay, resulting in modifications to the tidal amplitude and phase, in addition to the generation of overtides and compound tides [Aubrey and Speer (1985); Friedrichs and Aubrey (1988); Friedrichs et al. (1992); Speer et al. (1991)]. Changes in the geometry of an inlet (i.e., physical dimensions and orientation) are well known to alter the sea level and circulation patterns within the inlet and bay, and can alter the role of advection as currents follow different paths [Aubrey and Speer (1985); Friedrichs and Aubrey (1988); Speer et al. (1991)]. Changes in hydraulic radius (cross-sectional area divided by wetted perimeter) and inlet length also can alter the role of friction. For example, as an inlet lengthens, narrows, and shoals, the forcing tides are increasingly restricted, retarding flows into and out of the bay, and thus affecting the circulation within the bay. Both advective and frictional changes affect the propagation of the tide, and in particular generate higher-frequency motions from nonlinear interactions between motions of the primary tidal constituents [Aubrey and Speer (1985); Blanton et al. (2002); Friedrichs and Aubrey (1988); Friedrichs et al. (1992); Le Provost (1991); Parker (1991); Speer and Aubrey (1985); Speer
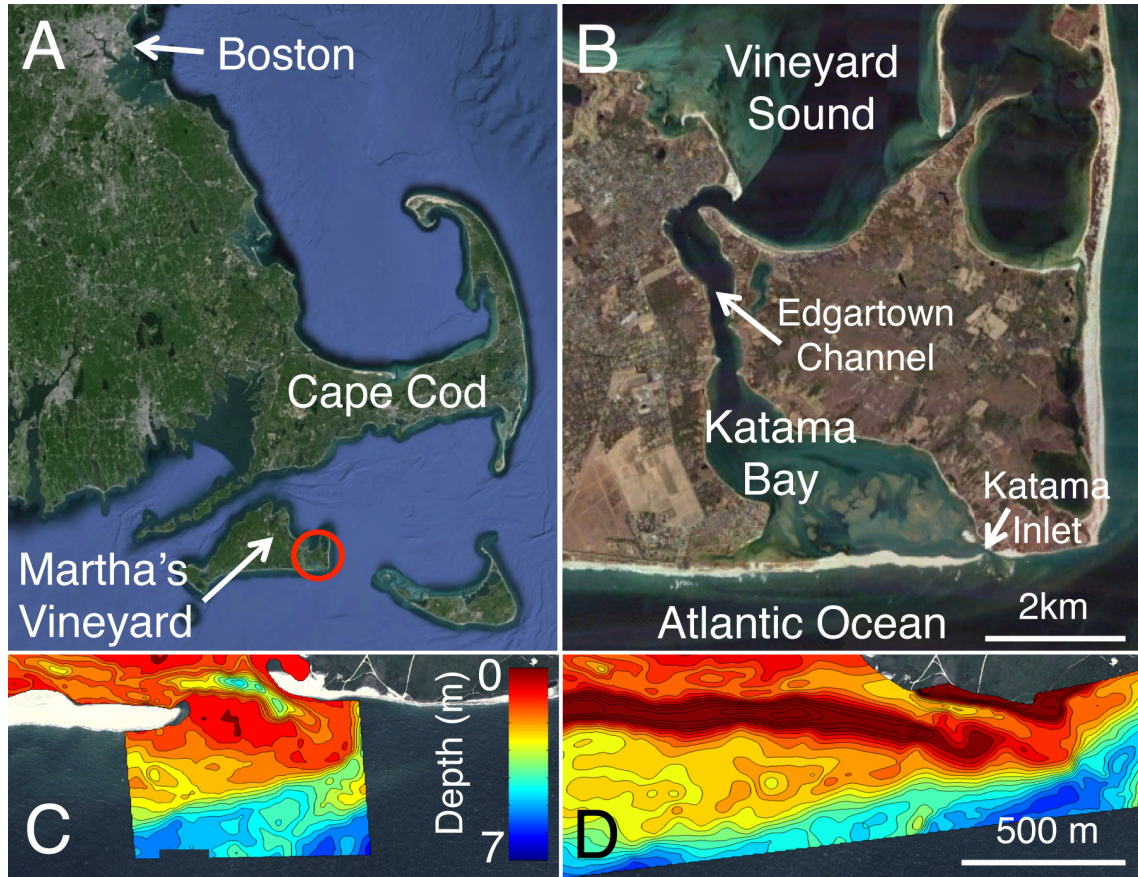
Figure 3-1: Google Earth images of (A) location of Martha's Vineyard, MA, with the Katama system inside the red circle, and (B) Katama Bay showing Edgartown Channel to the north and Katama Inlet to the south. Bathymetry (color contours, scale on the right) near the mouth of Katama Inlet observed in (C) September 2011 and (D) July 2013 (dark red contours in D are subaerial). The color bar in (C) and the scale bar in (D) apply to both (C) and (D).

et al. (1991)]. Assuming a shallow, well-mixed, irrotational system, conservation of mass and momentum in one direction can be expressed as [Parker (1991)]:

$$\frac{\partial \eta}{\partial t} = \frac{\partial}{\partial x} \left( (h + \eta) \, u \right) \tag{3.1}$$

and,

$$\frac{\partial u}{\partial t} + u \frac{\partial u}{\partial x} = -g \frac{\partial \eta}{\partial x} - C_d \left( \frac{1}{h + \eta} \right) u |u| \tag{3.2}$$

where $\eta$ is the water level relative to mean sea level, $t$ is time, $x$ is the spatial coordinate, $h$ is the mean water depth, $u$ is the depth-averaged velocity, $g$ is gravitational acceleration, and $C_d$ is a drag coefficient for quadratic friction. To analyze the nonlinear effects of these equations, the friction term can be expanded assuming $\eta^2 \ll h^2$ to:

$$C_d \left( \frac{1}{h + \eta} \right) u |u| \cong \frac{C_d}{h} \left( 1 - \frac{\eta}{h} \right) u |u| \tag{3.3}$$

yielding two separate terms for frictional effects. The absolute value operator results in a doubling of the frequencies of the components of the tidal time series.

The nonlinear terms describing the advection of mass, $\partial(\eta u)/\partial x$, and momentum, $u \partial u/\partial x$, generate even harmonics of the driving motions. For example, terms with two or more time-dependent variables can generate harmonics or overtides depending on the number of varying parameters ($u$ and $\eta$ in Equations 3.1 and 3.2). Specifically, advection generates motions primarily at the second harmonic, M4 of an M2 driving tide. Some of the effects of friction, specifically from $-(C_d/h^2)\eta u |u|$, produce even harmonics owing to the absolute value operator. In this case, the lowest even harmonic generated is the 4th harmonic (e.g., M8 is generated from an M2 driving force). Usually, owing to the multiplication of decreasingly energetic harmonics, this higher-order interaction is relatively small. In contrast, the other frictional term, $(C_d/h)u |u|$, generates odd harmonics. For example, friction can generate motions at M6 from an M2 driving tide.

Thus, even harmonics (e.g., M4) are generated primarily from advection and odd harmonics (e.g., M6) are generated primarily by friction (Blanton et al. (2002); Parker (1991) and others). The harmonics can interact with the primary driving forces, as well as with each other, producing higher-frequency motions. However, usually these higher-order interactions are relatively small. As the geometry of an inlet system changes in time, the

49

advective and frictional distortion of the tide will change. For a system dominated by the M2 lunar tide, changes in advection should result in a change in energy at the M4 frequency, whereas changes in friction should result in a change in energy at the M6 frequency. Temporal changes in the M4 constituent observed in a one-inlet system have been used to infer changes in bathymetry [Malhadas et al. (2009)]. Here, observed and modeled M4 and M6 constituents are used to determine the relative roles of advection and friction as the inlet evolves and bay circulation changes.

## 3.4   Field measurements

The bathymetry from the northern end of Edgartown Channel through Katama Bay and Inlet and across the ebb shoal in the ocean to the south (Figures 3-1 and 3-2) was measured with a GPS- and acoustic-altimeter-equipped personal watercraft. The vertical resolution of the surveys is approximately 0.05 m, and the horizontal resolution is 0.10 m along transects separated by 5 m (near complex bathymetry) to 60 m (uniform bathymetry). Surveys were conducted both before (July 2011, not shown) and after (September 2011, Figure 3-1C) the passage of Hurricane Irene (29 August 2011) and in July 2013 (Figure 3-1D). The bay surface area is approximately 7.5 x 106 m$^2$, and water depths range from less than 1 m on the flood shoal to 10 m at the northern part of the Bay (Figure 3-2).

In 2011, Katama Inlet was a relatively short (200 m), wide (400 m), and deep (4.0 m) inlet oriented roughly north-south (Figures 3-1C and 3-2A). There was a prominent ebb shoal offshore of the inlet mouth, and a large flood shoal intersected by channels on the bay side of the inlet. By 2013, Katama Inlet (and the ebb shoal) had migrated over 1000 m to the east, rotated to a nearly east-west orientation, elongated (1000 m), narrowed (150 m), and shoaled (1.5 m depth) (Figures 3-1D and 3-2B). By February 2015 the sand barrier separating the bay from the ocean had extended to the eastern edge of Chappaquiddick Island, and the inlet had increased another 700 m in length (not shown). On 1 April 2015, the inlet closed.

Water levels and currents were observed from 1 to 30 September 2011 and from 1 to 26 August 2013. Sea-surface elevation fluctuations were measured (2 Hz samples) with buried pressure gauges deployed along and across the bay and inlets (Figure 3-2). The pressure time series were corrected for atmospheric pressure fluctuations. There is an approximately
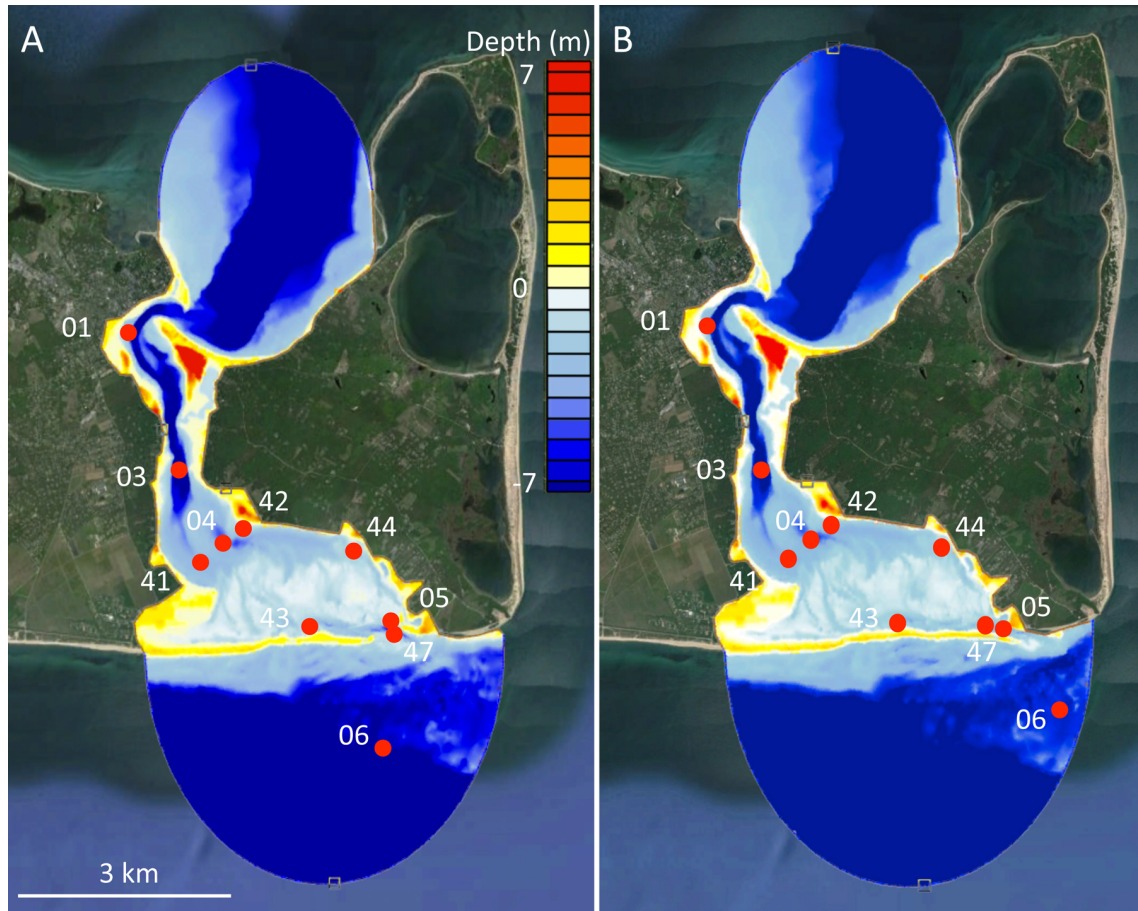
Figure 3-2: Model domain (color contours are elevation relative to mean sea level) and sensor locations (red symbols) during (A) 2011 and (B) 2013. Sensor 01 is a pressure gauge, sensors 05, 06, and 44 are single point acoustic current meters, and all other sensors are acoustic current profilers. Pressure gauges were colocated with each current meter and profiler. The Martha's Vineyard Coastal Observatory is located about 7 km west of the inlet in 12-m water depth.

3-hr phase lag between the M2 tidal constituent in Vineyard Sound and the M2 tide in the ocean (Chen et al., 2011), producing tidally varying pressure gradients from the up to 1-m difference in sea-surface elevation across the 7-km long Katama system.

The pressure gradients drive strong currents, which were measured with profiling acoustic current meters (Figure 3-2) and single-point acoustic Doppler velocimeters. The profilers estimated 1-min mean currents in 0.25-m (for sensors in less than 10-m water depth) and 0.50-m ($> 10$ m depth) high vertical bins from 0.25 m above the seafloor to the surface. Velocimeters were deployed in water too shallow for profilers (sensor 44 in Figure 3-2), and on the ebb shoal (sensor 06) and in the inlet (sensor 05) to estimate wave properties (2 Hz samples).

There is no source of fresh water to Katama Bay, and many CTD casts throughout the system showed there was little vertical variation in temperature or salinity (32 PSU). Similarly, there was little vertical variation in mean currents, and thus depth-averaged 10-min mean velocities are considered here. Wind was measured on the Martha's Vineyard Coastal Observatory (`MVCO:http://www.whoi.edu/mvco`) 12.5-m-tall meteorological mast on South Beach, Martha's Vineyard, a few km west of Katama Inlet (not shown).

## 3.5   Model

The numerical hydrodynamic model ADCIRC [Luettich and Westerink (1991); Luettich et al. (1992)] was implemented for the Katama system. The two-dimensional depth-integrated (2DDI) version of ADCIRC solves the continuity and momentum equations, including all nonlinear terms, using finite elements on flexible, unstructured grids that allow for high spatial resolution of spatially varying geometries, such as the complex bathymetry near inlets. The depth-integrated continuity equation is:

$$\frac{\partial \eta}{\partial t} + \frac{\partial U H}{\partial x} + \frac{\partial V H}{\partial y} = 0 \tag{3.4}$$

where $x$ and $y$ are the horizontal coordinates, $U$ and $V$ are depth-integrated velocities and $H = h + \eta$ is the total water depth. Similarly, the momentum balances are:

$$\frac{\partial U}{\partial t} + U\frac{\partial U}{\partial x} + V\frac{\partial U}{\partial y} - fV + g\frac{\partial \eta}{\partial x} - \nu\nabla^2 U + \left(\frac{C_d\sqrt{U^2 + V^2}}{H}\right)U = 0 \tag{3.5}$$

and

$$\frac{\partial V}{\partial t} + U\frac{\partial V}{\partial x} + V\frac{\partial V}{\partial y} + fU + g\frac{\partial \eta}{\partial y} - \nu\nabla^2 V + \left(\frac{C_d\sqrt{U^2 + V^2}}{H}\right)V = 0 \qquad (3.6)$$

where $f$ is the Coriolis parameter, $\nu$ is the lateral eddy exchange coefficient and $C_d$ is the quadratic bottom friction coefficient. ADCIRC solves Equations 3.4 - 3.6 numerically Luettich et al. (1992) and was chosen here to model the well-mixed Katama Bay system because finite elements are good for complex bathymetry. In addition, ADCIRC simulates wetting and drying, which can be important to circulation in small bays with tidally varying shorelines owing to the change in bay surface area.

The model bathymetries (Figure 3-2) consisted of the watercraft surveys in 2011 and 2013, supplemented with the 2008 Nantucket 10 m resolution DEM (`www.ngdc.noaa.gov`) in Vineyard Sound and the Atlantic outside the ebb shoal. To account for the effects of wetting and drying, the model requires high-resolution surveys near the shoreline, especially in gently sloping areas where there is significant change during a tidal cycle. In deeper water, especially where the bathymetry is relatively smooth, less dense surveys are sufficient. Model grid resolution was 10 m within Katama Inlet and 30 m elsewhere. Using a 10-m resolution grid everywhere did not change the results.

To keep the model domain small and to compare model results with observations, the simulations are driven at the northern and southern boundaries by the sea-level fluctuations observed in the sound and in the ocean, thus accounting for the complex propagation of tides into the area, as well as the effects of wind and atmospheric pressure on water levels. Specifically, pressure measurements made at Sensor 01 (Figure 3-2) and at the Martha's Vineyard Coastal Observatory (MVCO) 12-m node (`http://www.whoi.edu/mvco`) were used for the northern and southern boundaries, respectively. The pressure time series are used in lieu of tidal constituents owing to the complex tides in the region, especially Vineyard Sound. Although breaking waves can drive water into the inlet affecting circulation throughout the bay [Malhadas et al. (2009); Orescanin et al. (2014); Wargula et al. (2014)], waves were relatively small for the data considered here and are not included in the model. Similarly, although the wind effects on mean water levels are included in the boundary conditions, winds usually were light and the bay surface area is small so wind stress over the bay is neglected.

In the southern part of the domain, water levels were measured in the ocean (at MVCO),

near the boundary (Figure 3-2). However, in the northern part of the domain, water levels were measured in Edgartown Harbor (northern-most sensor in Figure 3-2), some distance from the boundary in the sound. Thus, to drive the model at the northern boundary the amplitude of the time series of water level observed in Edgartown Harbor (at sensor 01) were increased by 18% so that the simulated water levels in the harbor matched the observed water levels. There was no need to adjust the phase of the Edgartown water levels when applied on the northern boundary.

Drag coefficients at Edgartown Channel ($C_d$=0.007) and Katama Inlet ($C_d$=0.011) estimated from the observations (Orescanin et al., 2014) were used to select Manning's $n$ (where $C_d = gn^2h_c^{-1/3}$) for Edgartown Channel and Katama Bay ($n$=0.030) and for Katama Inlet ($n$=0.035). In the sound and ocean, $n$=0.020, the value typically used for deeper water. The results are not sensitive to 15% changes in the values of $n$ or to using a spatially constant value of $n$=0.030. However, the spatially variable Manning's $n$ minimizes the overall error in energy throughout the system.

The model is forced with observed sea-surface elevation time series on the boundaries, and is run with a 0.5 s time step for numerical stability, with a one-day spin up from the initial boundary conditions and an initial flat sea surface over the entire domain. Lateral viscosity is set to 2.0 m$^2$/s. Here, snapshots every 20 minutes of model simulations of sea-surface elevation and depth-averaged velocities are compared with 20-min averages of observed sea-surface elevation and depth-averaged velocities. Other averaging schemes did not change the results.

## 3.6   Model-data comparisons

The model skillfully simulates the sea-surface elevation fluctuations observed in Katama Inlet. In both 2011 (Figure 3-3A) and 2013 (Figure 3-3D) sea level is predicted accurately during spring and neap tides. The (relatively small) model errors during neap tide 16 to 18 Sep 2011 (Figure 3-3A) could be caused by neglect of the effects of 3-m high offshore (12-m water depth) waves during a nor'easter storm that peaked on 16 Sep.

The model also skillfully simulates the velocities observed along the major flow axes in Katama Inlet in both 2011 (Figure 3-3B) and 2013 (Figure 3-3E). In contrast, the model does not predict the strength of the minor-axes flows observed in Katama Inlet in 2011
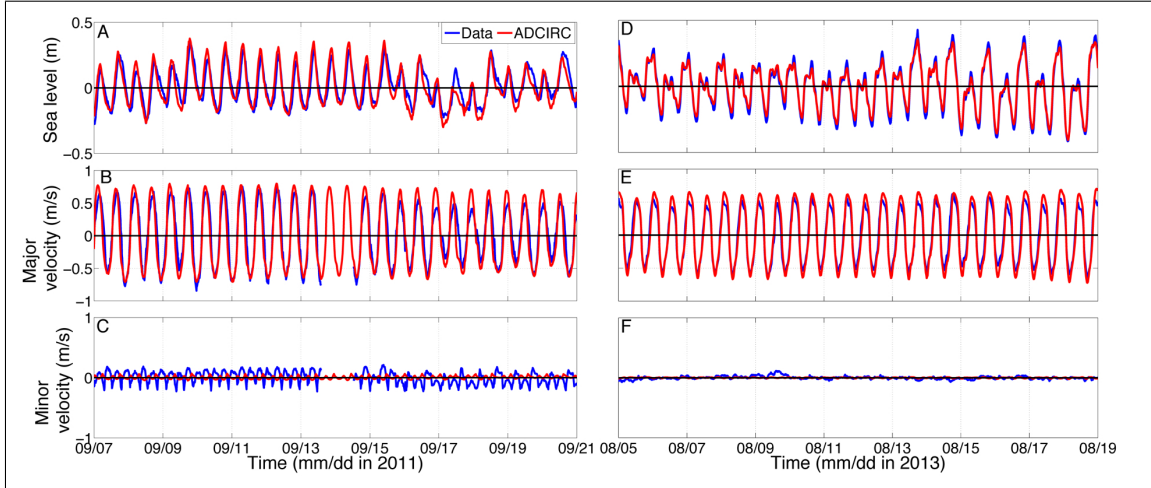
Figure 3-3: Observed (blue curves) and modeled (red curves) (A and D) sea-surface elevation, and (B and E) major and (C and F) minor-axis depth-averaged velocities in Katama Inlet (sensor 05, Figure 3-2) versus time in 2011 (A-C) and 2013 (D-F).

(Figure 3-3C). Although relatively weak compared with the major-axes flows, the observed minor-axes flows are stronger than predicted, possibly owing to unmodeled processes, such as alongshore propagation of the tide on the boundaries [Van Leeuwen and De Swart (2002)], sea breezes, the passage of weak fronts that can force water across the inlet channel, or 3D effects, as well as to incorrect model bathymetry.

The doubling of the frequency of the observed minor-axis flows at Katama Inlet in 2011 (Figure 3-3C) is caused by flow curvature around the spit near the sensor (Figures 3-1C and 3-2A) that results in similar east-west components of the flow during ebb (toward south east) and during flood (toward the north east). In 2013 the inlet geometry and the sensor location differed from those in 2011, and both the observed and simulated minor-axis flows were negligible (Figure 3-3F), possibly because the significantly longer and narrower inlet in 2013 restricted cross-channel flow.

The model simulates sea levels and currents in Edgartown Channel and throughout the Bay with similarly high skill for both September 2011 and August 2013 (Figure 3-4). Modeled major-axis flows are somewhat stronger than observed, and modeled minor-axis flows are somewhat weaker than observed (compare colored with black ellipses in Figure 3-4A,B, and compare the circles with triangles representing the energy of the currents in Figure 3-4C), likely owing to unmodeled processes listed above.

Observed and modeled maximum currents in Edgartown Channel and Katama Bay were
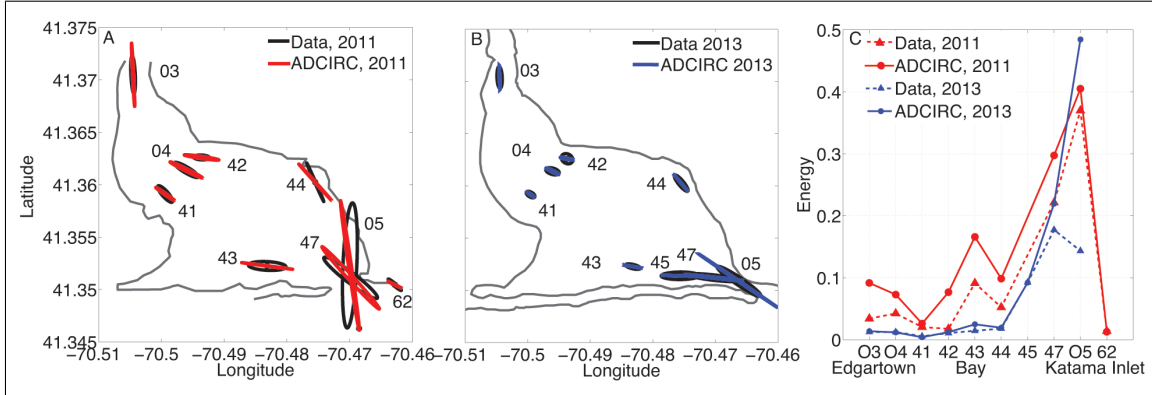
Figure 3-4: Observed (black) and modeled (red and blue) principal flow axes in (A) 2011 (red) and (B) 2013 (blue). (C) Total velocity energy (minor-axis-velocity$^2$+ major-axis-velocity$^2$) at each sensor location versus sensor number (locations are listed near each ellipse in A and B). Triangles are observations (connected by dashed lines) and circles are model predictions (connected by solid lines). Sensor 62 was near the surfzone outside the inlet. The amplitudes of observed major-axis velocities at sensor 05 were approximately 0.6 (2011) and 0.4 (2013) m/s.

significantly smaller in 2013 than in 2011 (compare ellipses in Figure 3-4A with those in 3-4B), and the overall kinetic energy of the currents (minor-axis-velocity$^2$ + major-axis-velocity$^2$) decreased by as much as 2/3 (Figure 3-4C). Model simulations suggest the reduction in currents from 2011 (Figure 3-5A,B) to 2013 (Figure 3-5C,D) occurs over most of the domain, except within some parts of Katama Inlet. Although the strength of the circulation decreases as the inlet evolves, the spatial patterns of the currents remain qualitatively similar during both flood and ebb flows (Figure 3-5).

## 3.7   Discussion

Although the long-term (few years) evolution of Katama Inlet has resulted in a loss of velocity energy throughout the Katama system (Figure 3-4C), the change has not been monotonic. For example, Hurricane Irene impacted the Katama system in late August 2011, resulting in significant changes to the inlet bathymetry, including areas with $> 2$ m of erosion or accretion (Figure 3-6). The model run with pre- and post-storm bathymetry and forced with the same 4-week-long time series of observed tidal levels in the sound and ocean suggests the bathymetric changes result in an increase of current speed (energy) throughout the bay (Figure 3-7). The model could be used to simulate bay circulation for other geometries, such
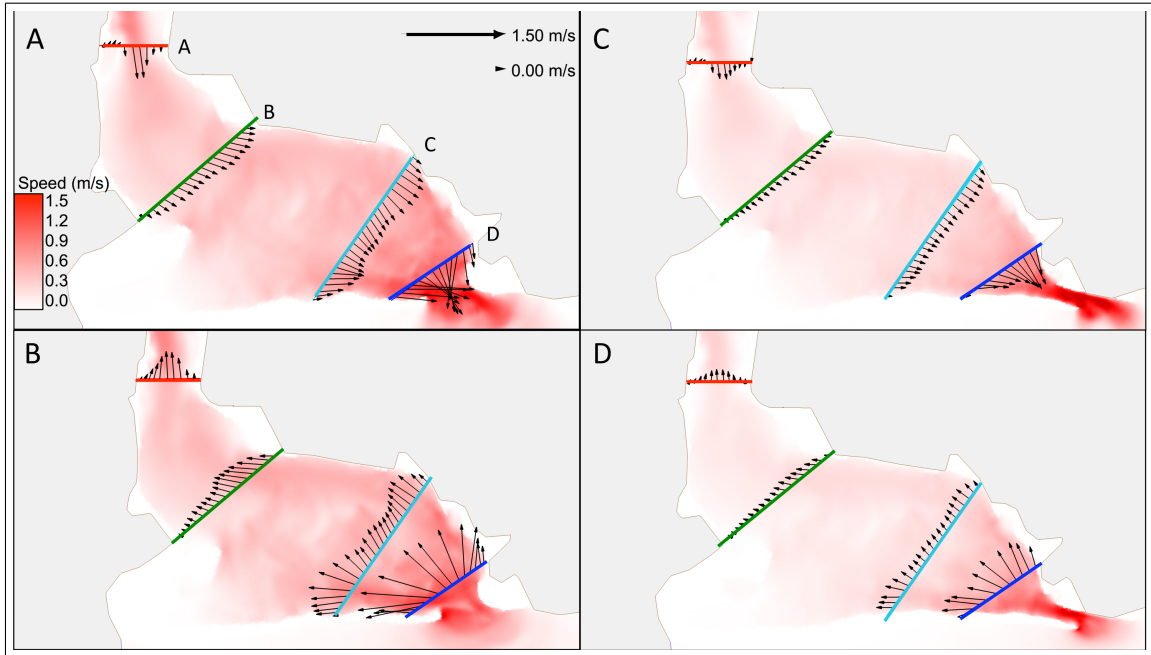
Figure 3-5: Model simulations of velocity magnitude (color contours and length of arrows) and direction (direction of arrows) during (A and C) ebb and (B and D) flood flows in (A and B) 2011 and (C and D) 2013. Scales are shown in (A).

as with a wide inlet in the center of Norton Point (similar to the inlet immediately after the breach in 2007) or no inlet.

As the inlet evolved between 2011 and 2013, the tidal constituents of both the observed (Figure 3-8A) and simulated (not shown, similar to the observations) sea-surface elevation time series in Edgartown Channel did not change significantly, and are similar to those in Vineyard Sound (not shown). In contrast, the M4 and M6 constituents of the velocity magnitude (primarily major-axis flows), as well as the ratio of these constituents to the M2 constituent, increased from 2011 to 2013 (Figure 3-8B). The relatively larger increase in the M6 component suggests a larger role of changes in friction than in advection. The model under predicts the observed levels of the M4 and M6 velocity fluctuations (not shown), but the trend from 2011 to 2013 is similar to that observed (Figure 3-8B).

In Katama Inlet, the 2011 and 2013 M4 components of the observed and simulated (not shown) sea-surface elevation are similar to each other (compare red with blue circles in Figure 3-9A), and are much larger than in the ocean (black in Figure 3-9A). The relatively large M4 component suggests advection is important near the inlet. Although the M4 component of sea-surface elevation in the inlet did not change as the inlet evolved (compare
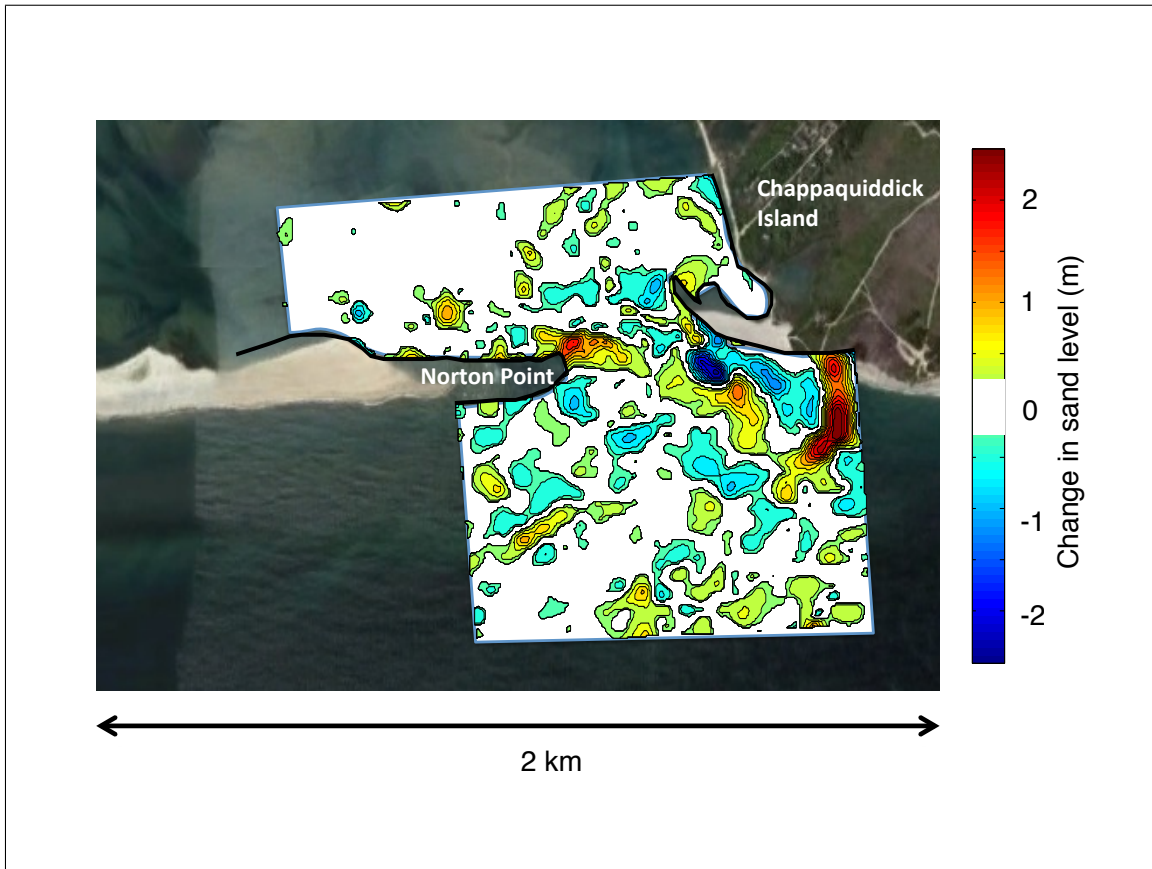
Figure 3-6: Contours of bathymetric change between 1 month before and 1 month after the passage of Hurricane Irene, 29 Aug 2011. Red is accretion, blue is erosion (scale on the right). Changes less than 0.25 m are not shown. The inlet channel migrated eastward (to the right) and in some locations became deeper.
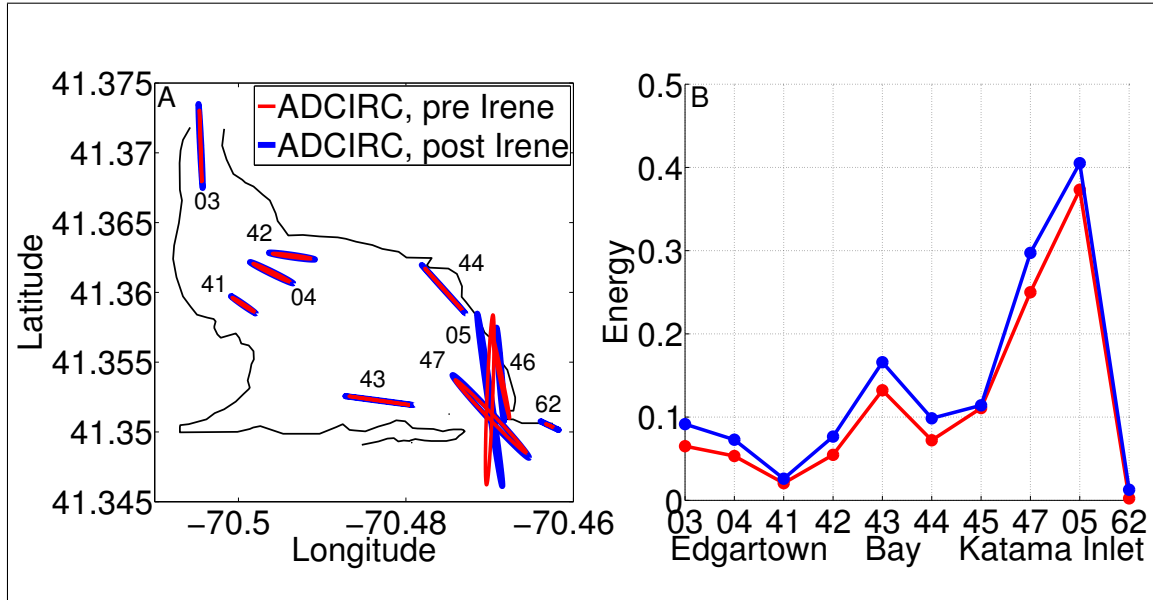
Figure 3-7: (A) Modeled principal flow axes before (red) and after (blue) Hurricane Irene, 29 August 2011 and (B) total velocity energy (minor-axis-velocity$^2$ + major-axis-velocity$^2$) at each sensor location versus sensor number (locations are listed near each ellipse in A). Blue (pre-Irene) and red (post-Irene) lines connect predictions at the locations of the sensors. The amplitudes of major-axis velocities at sensor 05 were approximately 0.6 m/s.

red with blue in Figure 3-9A), the M6 components of observed and simulated (not shown) sea-surface elevation are similar to those in the ocean in 2011 (compare red with black in Figure 3-9A), and their ratio to the M2 component increases by a factor of 3 or more in 2013 (compare blue with red in Figure 3-9A). Similar to sea-surface elevation, the M6 component of velocity at Katama Inlet increases from 2011 to 2013 (compare blue with red in Figure 3-9B), whereas the M4 component decreases between 2011 and 2013 (Figure 3-9B). The observed and modeled (not shown) decrease in M4 and the increase in the M6 component as the inlet evolved between 2011 and 2013 are consistent with a decreasing relative importance of advection and an increasing relative importance of friction as the inlet became longer, narrower, and shallower.

To test the effect of increased friction without changing the inlet geometry, the model was run with the 2011 bathymetry and boundary forcing conditions, but with Manning's $n$ increased to $n = 0.085$ within Katama Inlet. The resulting circulation patterns are similar to those observed and modeled in 2013 with $n = 0.035$ (Figure 3-10), and are significantly less energetic than in 2011 (dashed lines in Figure 3-10B), suggesting that the differences in
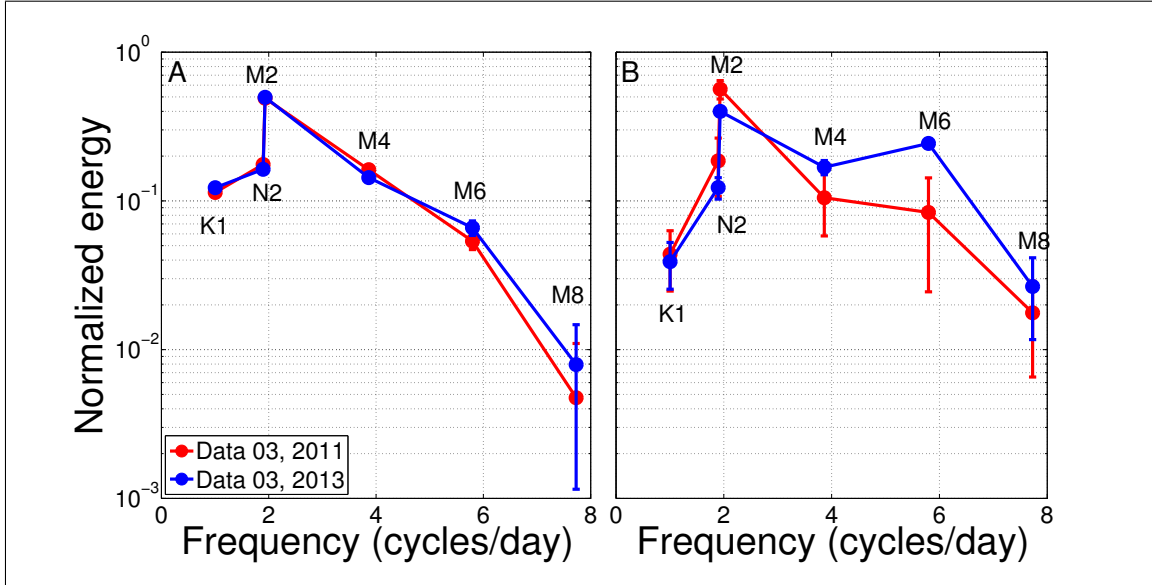
Figure 3-8: Normalized (by the total energy) energy density versus frequency of the largest (approximately 90% of the total energy) tidal constituents from observations in Edgartown Channel (sensor 03 in Figure 3-2) of (A) sea-surface elevation and (B) velocity magnitude (predominantly major-axis flow, Figure 3-3). Constituent (labeled in each panel) energy and 1 standard deviation error bars were estimated using t_tide [Pawlowicz et al. (2002)] from approximately 1-month long time series.

circulation in the bay are primarily the result of increased friction in the 2013 inlet. The increase in frictional damping as the inlet lengthens has been hypothesized to contribute to the inlet closure [Ogden (1974)].

Although the tidal constituents of both velocity (Figures 3-8B and 3-9B) and sea-surface elevation (Figures 3-8A and 3-9A) are consistent with an increased role of friction, there are significant differences in the spectra. Unlike a single progressive wave, for which the velocity is in phase with the sea-surface elevation [Aubrey and Speer (1985); Dronkers (1986); Friedrichs and Aubrey (1988); Friedrichs et al. (1992)] or a standing wave (caused by reflection of the tide), for which velocity is in quadrature (90° phase difference) with sea-surface elevation [Broenkow and Breaker (2005); Thornton et al. (submitted)], in the Katama system there are two waves propagating in opposite directions, and possibly partially reflecting and dissipating. For example, the phases between sea-surface and velocity fluctuations in the observations at M2 in 2011 and 2013 at Edgartown were 33° and -4° and at Katama were -55° and 49°, respectively (The coherence between M2 sea-surface elevation and velocity is high.). Thus, the total tide (M2 and constituents) may consist of multiple waves, and
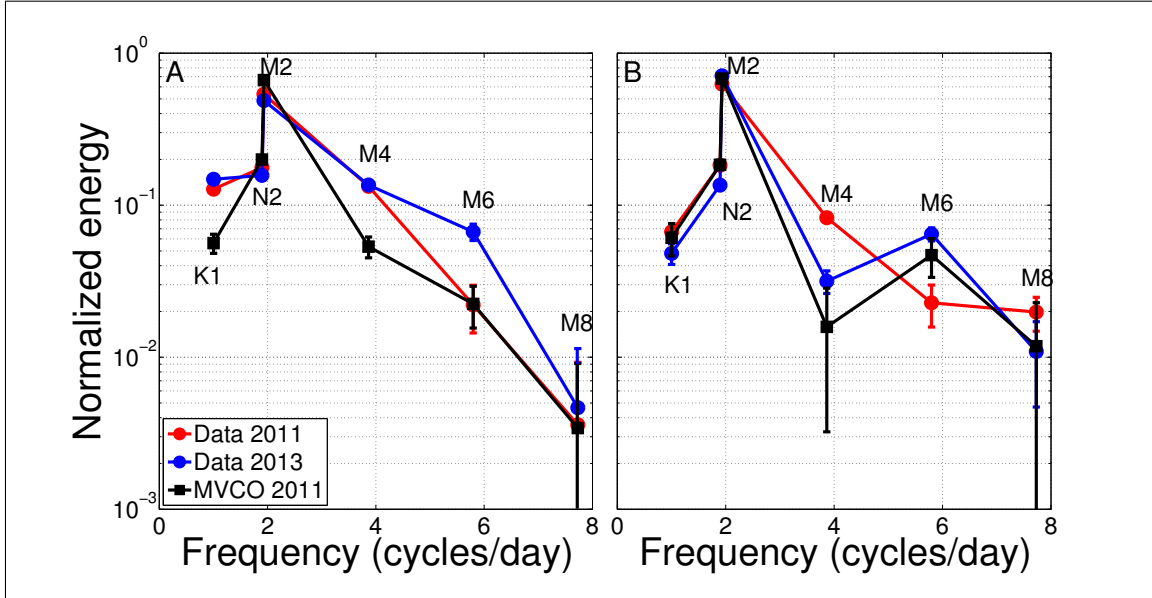
Figure 3-9: Normalized (by the total energy) energy density versus frequency of the largest (approximately 90% of the total energy) tidal constituents from observations at the Martha's Vineyard Coastal Observatory (MVCO, black, 2011) and in Katama Inlet (sensor 05 in Figure 3-2, red 2011 and blue 2013) of (A) sea-surface elevation and (B) velocity magnitude (predominantly major-axis flow, Figure 3-3). Constituent (labeled in each panel) energy and 1 standard deviation error bars were estimated using t_tide [Pawlowicz et al. (2002)] from approximately 1-month long time series.

shapes of sea-surface elevation fluctuations are not necessarily related to shapes of velocity fluctuations. For example, although observed and modeled sea-surface elevation skewness [the mean of the cube of the demeaned time series normalized by the variance raised to the 3/2 power (Elgar and Guza (1985); Nidzieko (2010) and many others) at Edgartown was negative in both 2011 and 2013 (not shown), implying flood dominance for the sign convention used here [Nidzieko (2010)], velocity skewness was not significantly different than 0 (not shown). Similarly, although sea-surface elevation skewness at Katama is positive in 2011 and negative in 2013 (Figure 3-11B), implying a change from flood to ebb dominance, observed velocity skewness is not statistically different than 0 in either year (Figure 3-11C).

Skewness describes asymmetries of the time series about the horizontal axis (e.g., wave crests are shaped differently than troughs), and skewed velocities can lead to net sediment transport (Bagnold (1966); Bailard (1981); Bowen (1980) and many others). Similarly, velocities that are asymmetrical about a vertical axis (front and rear faces of the wave differ) [Elgar and Guza (1985); Kim and Powers (1979); Masuda and Kuo (1981); Nidzieko
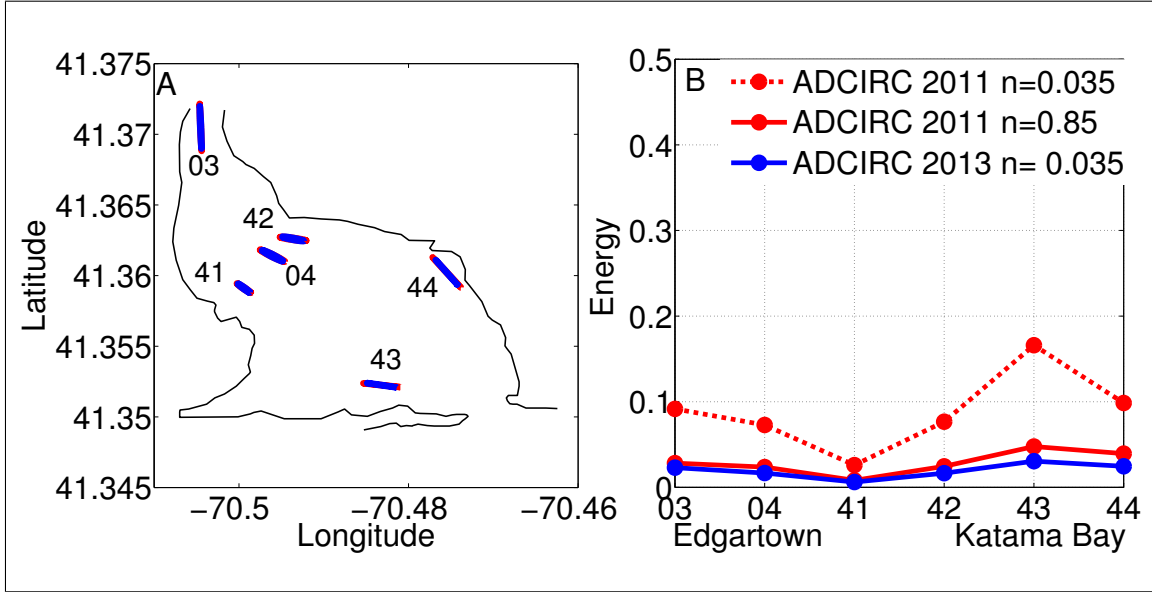
Figure 3-10: (A) Modeled principal flow axes using the 2011 bathymetry with Manning's $n$ = 0.085 (red) and the 2013 bathymetry with $n$ = 0.035 (blue). Both model runs use the same boundary conditions. (B) Total velocity energy (minor-axis-velocity$^2$ + major-axis-velocity$^2$) at each sensor location versus sensor number (locations are listed near each ellipse in A). Solid red ($n$=0.085, 2011 bathymetry), blue ($n$=0.035, 2013 bathymetry), and dashed red ($n$=0.035, 2011 bathymetry) lines connect predictions at the locations of the sensors. The amplitudes of modeled major-axis velocities at sensor 03 were approximately 0.3 m/s in 2011 and 2013.

(2010)] also can transport sediment [Drake and Calantoni (2001); Hoefel and Elgar (2003)]. This asymmetry is described by the skewness of a 90° phase-shifted version (the Hilbert transform) of the time series (called "asymmetry", [Elgar and Guza (1985)], similar to the "duration skewness" [Nidzieko (2010); Nidzieko and Ralston (2012)]). Here, sea-surface elevation and velocity asymmetry at Edgartown were not different than 0 (not shown), but at Katama sea-surface elevation asymmetry went from positive to zero (Figure 3-11B), while velocity asymmetry went from negative to positive (Figure 3-11D), consistent with a change from flood to ebb dominance between 2011 and 2013, possibly contributing to the inlet closure in 2015.

## 3.8   Conclusions

Observations and numerical simulations show that the circulation in Katama Bay became less energetic between 2011 and 2013, primarily owing to increased frictional losses as the
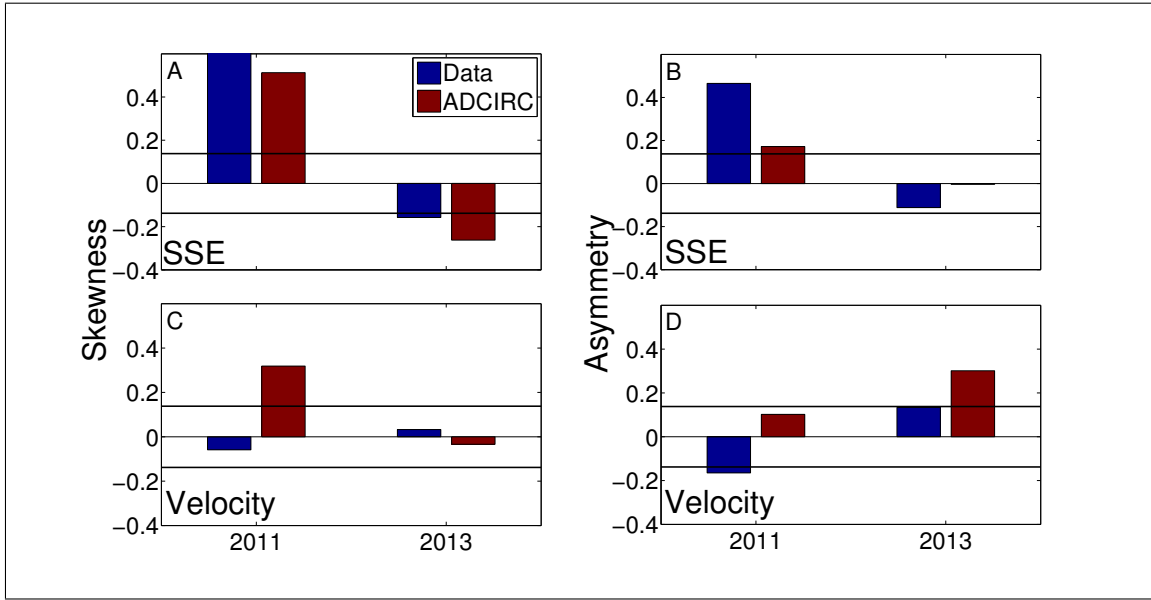
Figure 3-11: (A and C) Skewness and (B and D) asymmetry of observed (blue) and modeled (red) sea-surface elevation (A and B) and velocity (C and D) at Katama Inlet for 2011 and 2013. For a random process with the same number of degrees of freedom as the observations, skewness and asymmetry (absolute) values greater than 0.14 (the thick horizontal lines) are statistically greater than 0 at the 90% level. Skewness is the mean of the cube of the time series normalized by the variance to the 3/2 power, and asymmetry is the mean of the cube of the Hilbert transform (a 90° phase shift) of the time series normalized by its variance to the 3/2 power.

inlet channel lengthened, narrowed, and shoaled. The model (2DDI-ADCIRC) suggests that the 2-yr trend of decreasing currents was not monotonic. For example, bathymetric changes caused by the passage of Hurricane Irene resulted in stronger modeled currents than before the hurricane. As the inlet geometry changed, the M4 harmonic (associated with advection) of the primary M2 tide did not change, while the M6 component increased, consistent with increased friction. As Katama Inlet evolved, the flows in Edgartown Channel remained flood dominant, whereas the velocity skewness and asymmetry at Katama Inlet suggest flows changed from flood to ebb dominant. Closure of the inlet (in 2015) may have resulted from the combination of frictional damping of the flows and the change from flood to ebb dominance.

# Chapter 4

# A Hydrodynamic Lumped-Element Model for Tidal Inlets and the Effect of a Shallow Bay

## 4.1 Abstract

The effect of a shallow flood shoal on the hydrodynamics of a multi-inlet system are quantified through a lumped element (parameter) model that determines the complex impedance of the inlet-bay system caused by impedances owing to inlet and bay dimensions, friction, and the depth mismatch between the inlet and the bay. This approach allows the bay circulation to be determined for any configuration of small inlet(s) and bay(s), and quantifies the geometric affects of inlet dimensions on back bay circulation. Results indicate that for the evolving two-inlet system of Katama Bay, Martha's Vineyard, MA, the tidal sea-surface amplitude in the bay is not sensitive to changes in the relative size of the step between Katama Inlet (connects the bay to the Atlantic Ocean) and the bay (the ratio of the difference in depth between the deeper inlet and the shallower bay to the depth in the inlet). In contrast, the phase of the tidal sea-level fluctuations in the bay relative to that in Edgartown Channel (connects the bay to Vineyard Sound) is affected by the relative size of the step. In addition, as the ratio of inlet length to cross sectional area increased from 2011 to 2014, the lumped element model suggests an increasing importance of friction relative to the importance of the step, consistent with observations and previous numerical model results.

## 4.2 Introduction

Many studies of both single- and multiple-inlet systems assume that the back bay is deep relative to the tidal range and that the length scales of the bay are small relative to the wavelength of the tide [Keulegan (1967); O'Brien and Clark (1974); Maas and Doelman (2002); and many others]. Thus, the depth of the back basin has little effect on the hydrodynamics. There have been studies that examine the presence of topographic highs within the back basin [Maas (1997); Stanev et al. (2003); Herman (2007); van de Kreeke et al. (2008); Waterhouse et al. (2011); De Swart and Volp (2012)]. However, these studies do not examine the effects of a topographic high located where the inlet joins the back bay. In particular, it is expected that an abrupt change in bathymetry from a relatively deep inlet to a shallower bay within the area of strong flows from the inlet will affect the circulation by impeding the propagation of the tide into the bay.

Other studies of tidal inlet systems have considered a back bay connected by single or multiple inlets to the ocean to be analogous to a Helmholtz resonator [Miles (1971); Miles and Lee (1975); Maas (1997); Maas and Doelman (2002); Stanev et al. (2003)]. In this analogy, the volume of water in the inlet is the oscillating mass, and the natural frequency of the system is dependent on the geometry of the inlet and surface area of the bay. Similar to many studies, the back bay is assumed to be deep such that it does not affect the flow through the inlet.

Here, inlet impedance and the effect of the impedance mismatch between the inlet and back bay owing to depth differences between the regions is investigated with a new lumped element (parameter) model. The method presented here geometrically lumps parameters into inlet or bay components to predict the sea level response in the back bay. The solution to such a model is a simplified version of more generalized approaches [Miles (1971, 1974); Miles and Lee (1975)], and can be applied to any inlet and bay configuration for which the physical dimensions of each element are small relative to the wavelength of the driving force (the M2 tide here). The relative importance of each inlet, as well as the roles of friction and depth mismatch are considered under the assumption that frictional effects in the bay (where currents are weak) are small relative to those in the inlets (strong currents). Here, it is shown that a multiple-inlet system with an abrupt shoal at one inlet acts as a multiple-opening Helmholtz resonator with an additional impedance caused by the shallow

step, lessoning the effect of that inlet.

Lumped element modeling allows investigating the bulk (spatially averaged) properties of systems of field variables that are dependent on location and time, converting partial differential equations into ordinary differential equations [Pierce (1989)]. Common examples of such models are found in mechanical (spring-dashpot), acoustical (Helmholtz resonator), and electrical (RLC circuits) systems. For lumped element models, there are two variables associated with each element, one "across" the element and one "through" the element. For example, in the RLC circuit, the across variable is the voltage and through variable is the current. For a hydrodynamic system, the variable passing across the element is pressure (sea level) and the variable passing through the element is volume velocity (discharge).

Lumped element systems can provide computationally efficient, accurate estimates of phase-resolved sea levels and depth-averaged velocities within geometrically complicated systems. In addition, the lumped element approach allows the individual contributions (e.g., friction, advection, shallow bay) to the total impedance to be determined. By lumping the elements using physical dimensions of the inlet(s) and bay(s), this method shows the dimensional controls on the hydrodynamics of the system (e.g., changing the inlet length alters circulation within the entire system through changes in advection and friction).

Here, a new lumped element model for the two-inlet Katama system, including a sill or step where Katama Inlet enters the shallow bay, is developed. The model is compared with a linearized simple 1D momentum balance model [Orescanin et al. (2014)], and with field observations. Model simulations are used to investigate the changing relative roles of friction and of the step between (relatively) deep inlet and shallow bay as the inlet morphology evolved.

### 4.2.1   Previous Inlet Impedance Work

For a system for which the tidal amplitude is significantly smaller than the depths of the inlets and the back bay the restriction of water through an inlet and into a back bay is quantified by the repletion coefficient, $K$ derived from the continuity equation [Keulegan (1967)]:

$$K = \frac{T}{2\pi a_o} \frac{A_I}{A_B} \sqrt{\frac{2gra_o}{fL_I + nr}} \qquad (4.1)$$

where $T$ is the period of the forcing body of water, $a_o$ is the tidal amplitude, $A_I$ is the cross-sectional area of the inlet, $A_B$ is the surface area of the back bay, $g$ is gravity, $r$ is the hydraulic radius, $f$ is the Darcy-Weisbach friction factor (related to $C_d = f/4$, where $C_d$ is the drag coefficient), $L_I$ is the inlet length, and $n$ is an empirical constant for the shape of the flow (if uniform flow, $n=1$).

As $K \to 0$, there is no communication between the forcing body of water and the back bay, while $K \to \infty$ is the limiting case of no inlet present (i.e., the opening is as large as the bay). The repletion coefficient increases with $T$, the period of the forcing body of water, implying a dependence on the frequency of the driving tide.

Assuming a deep inlet and bay such that the tidal range is small relative to the depths, the impedance, $F$, of the inlet is defined as O'Brien and Clark (1974):

$$F = k_{en} + k_{ex} + \frac{fL}{4r} \tag{4.2}$$

where $k_{en}$ and $k_{ex}$ are entrance and exit losses at each end of the inlet. The term $F$ is the real component of the impedance, and is related to the repletion coefficient, $K$, by:

$$K = \frac{T}{2\pi a_o} \frac{A_I}{A_B} \sqrt{\frac{2gra_o}{F}} \tag{4.3}$$

If the bay and inlet depths are not large relative to the tidal amplitude there is additional impedance generated by the change in depth from the relatively deep inlet to the shallow bay.

## 4.3 Lumped Element Model for a Helmholtz Resonator and Single-Inlet System

A lumped element model for an inlet is derived by combining conservation of mass and momentum into a single equation for the sea level in the back bay. In doing so, it is possible to define the complex impedance of the system [Miles (1971, 1974); Miles and Lee (1975)]. Here it is assumed that the inlets and bay are small relative to the wavelength of the forcing body of water (tides here), Coriolis forces are negligible, the bay area does not change significantly (<20%) over a tidal cycle, and freshwater discharge and stratification are negligible. For a system with a rectangular bay and inlet, combining continuity and

momentum equations, and assuming linearized friction [Stanev et al. (2003); Terra et al. (2005); Malhadas et al. (2009)], yields:

$$\frac{d^2\eta_B}{dt^2} + \frac{C_d\overline{|u_I|}}{h_I}\frac{d\eta_B}{dt} + \frac{gA_I}{A_BL_I}\eta_B = \frac{gA_I}{A_BL_I}\eta_0 \tag{4.4}$$

where $\eta_B$ is the sea level in the bay, $t$ is time, $C_d$ is the drag coefficient, $\overline{|u_I|}$ is the mean of the absolute value of the depth- and width-averaged inlet velocity, $h_I$ is the depth of the inlet, $L_I$ is the length of the inlet, and $\eta_0$ is the sea level of the ocean. Equation 4.4 is a linearized version of Equation 2.1. Here, $A_B$ and all inlet dimensions are assumed to be constant, although there has been work to suggest the importance of incorporating the time variability of these parameters in locations where wetting and drying greatly alters the surface area of the bay over a tidal cycle [Speer and Aubrey (1985); Stanev et al. (2003); Terra et al. (2005); Herman (2007); De Swart and Volp (2012)]. The ordinary differential equation (4.4) has the same form as a damped driven harmonic oscillator and as a Helmholtz resonator (see (Kinsler et al., 1976) for an acoustic example).

Assuming a solution of the form $\eta \propto e^{j\omega t}$ Equation 4.4 becomes:

$$-\omega^2 e^{j\omega t} + j\omega\frac{C_d\overline{|u_I|}}{h_I}e^{j\omega t} + \frac{gA_I}{A_BL_I}e^{j\omega t} = \frac{gA_I}{A_BL_I}e^{j\omega t+\phi_0} \tag{4.5}$$

where $\omega$ is radian frequency, $\phi_0$ is the phase difference between the ocean and bay, and $j = \sqrt{-1}$. If $\eta \propto e^{j\omega t}$ is a solution, then so is $U \propto j\omega e^{j\omega t}$. Therefore, the complex impedance can be obtained for the single inlet system by multiplying Equation 4.5 by $\rho\frac{L_I}{A_I}$ (to get $P = \rho g\eta$) and dividing by $j\omega e^{j\omega t}$:

$$Z = \frac{P}{U} = j\omega\rho\frac{L_I}{A_I} + \frac{\rho C_d\overline{|u_I|}}{h_I}\frac{L_I}{A_I} + \frac{\rho g}{j\omega A_B} \tag{4.6}$$

This impedance is similar to that defined for the acoustical Helmholtz resonator: $Z = j\omega M + R + 1/(j\omega C)$, and allows for each element to be similarly defined for the inlet hydrodynamic system.

To define the elements for the lumped element model, and to define the complex impedance accordingly, the analogy to the Helmholtz resonator defines the oscillating mass as the mass of water within the inlet, and consequently the inertance, $M$ (similar to inertia in a momen-

tum balance) is given by:

$$M = \frac{m_I}{A_I^2} = \frac{\rho L_I A_I}{A_I^2} = \frac{\rho L_I}{A_I} \tag{4.7}$$

where $m_I = \rho L_I A_I$ is the mass of water in the inlet. Using the Helmholtz resonator form of the governing Equation (4.4) for the inlet system, the resistance $R$ (friction) is given by:

$$\frac{R}{M} = \frac{C_d \overline{|u_I|}}{h_I}$$

$$R = \frac{C_d \overline{|u_I|}}{h_I} \frac{\rho L_I}{A_I} \tag{4.8}$$

and the compliance, $C$, by:

$$\frac{1}{MC} = \frac{g A_I}{A_B L_I}$$

$$C = \frac{L_I A_B}{g A_I} \frac{1}{M} = \frac{L_I A_B}{g A_I} \frac{A_I}{\rho L_I} = \frac{A_B}{g \rho} \tag{4.9}$$

By defining the elements for the single inlet system, it is possible to re-write the complex impedance for this system as:

$$Z_{single\ inlet\ system} = j\omega M + R + \frac{1}{j\omega C} \tag{4.10}$$

which is the same as Equation (4.6) and that for the Helmholtz resonator or an electrical RLC circuit. Solving for the bay sea level of the inlet system (Figure 4-1A) is equivalent to solving for the voltage, $V_B$, in an electrical analog (Figure 4-1B) [Miles (1971, 1974); Miles and Lee (1975)]. The solution for the bay sea level is:

$$\eta_B(t) = U Z_C = \frac{Z_C}{Z_M + Z_R + Z_C} \eta_0(t) \tag{4.11}$$

where $U = \frac{\eta_0(t))}{Z_M + Z_R + Z_C}$ is the volume discharge velocity, $Z_C = \frac{1}{j\omega C}$ is the compliance of the bay, $Z_M = j\omega M$ is the inertance of the inlet, $Z_R = R$ is the resistance of the inlet, and $\eta_0(t)$ is the sea level in the ocean.
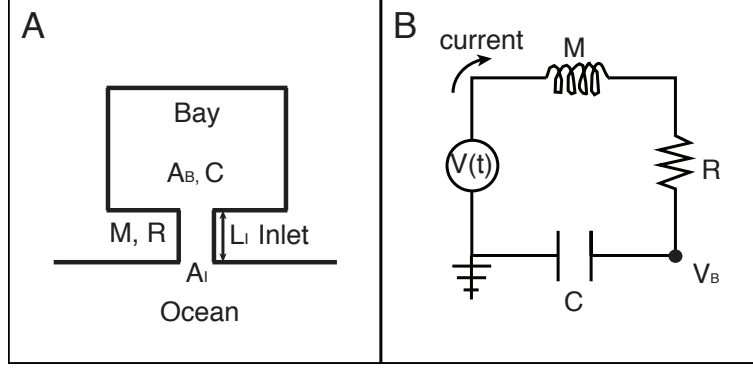
Figure 4-1: Schematic of A) a single inlet system with dimensions $A_I$ and $L_I$ forced by sea level in the ocean and B) the electrical representation for solving the governing equation for the single inlet system. The elements $M$, $R$, and $C$ in A) correspond to the electrical components in B). The solution for $\eta_B$ in A) is equivalent to the solution for $V_B$ in B), shown in Equation 4.11.

## 4.4 Lumped Element (Parameter) Model for a Multiple-Inlet System

The model for a single inlet-bay system can be expanded to include multiple inlets and bays. Given the elements defined for the inlet-specific inertance and resistance and the bay-specific compliance, an equivalent electrical circuit can be implemented that accounts for combinations of inlets and bays in series and parallel [Miles (1971); Miles and Lee (1975)], such as the Katama system (Figure 4-2). Different forcing can be applied at each inlet.

Unlike in systems with a deep bay, in shallow systems additional impedance is caused by a difference in depth between the inlet and the shallow flood shoal, modeled as a step. For the shallow depths considered here, the step-induced impedance $Z_S$ (Figure 4-2B) of each inlet is given by (see Appendix A for derivation):

$$Z_S = \frac{\rho c_B}{h_I b_I}\sqrt{\frac{h_B}{h_I}} - \frac{\rho c_B}{h_B b_I} = \frac{\rho c_B}{b_I h_B}\left(\frac{h_B^{3/2} - h_I^{3/2}}{h_I^{3/2}}\right) \tag{4.12}$$

where $c_B = \sqrt{gh_B}$ is the celerity of the tide in the bay. If $h_I = h_B$ then $Z_S \to 0$ (there is no impedance mismatch at the intersection of inlet and bay). If $h_B \to 0$ then $Z_S \to \infty$, because water cannot enter the bay through that inlet. As $h_B \to \infty$ the impedance to inlet flow is reduced.
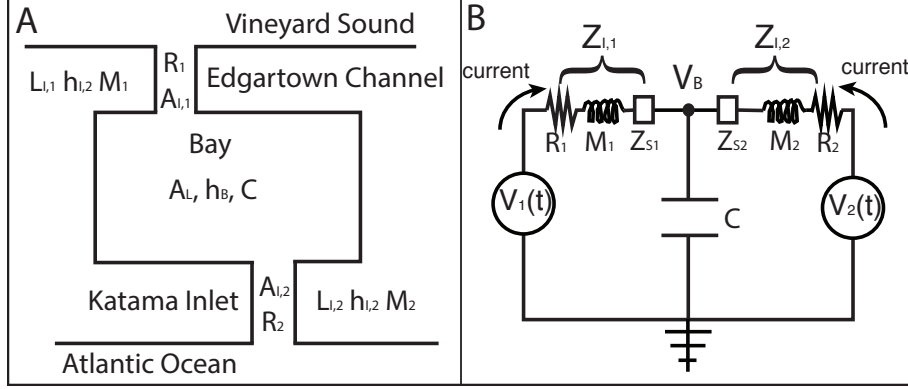
Figure 4-2: Schematic of A) double inlet hydrodynamic system and B) circuit analogy for the hydrodynamic system in A). Elements for lumped element (parameter) model are $C$, $M_1$, $M_2$, $Z_{S1}$, $Z_{S2}$, $R_1$, and $R_2$, where the subscripts refer to the specific inlet. The hydrodynamic system in A) is forced by sea levels in Vineyard Sound and the Atlantic Ocean, which are independent from each other. Similarly, the voltage forcings in B) are independent from each other. The voltage at $V_B$ in B) corresponds to the sea level in the bay in A). The element, $C$, related to the bay, couples the forcing from both inlets.

Similar to the one-inlet system with no depth mismatch, the other components of the inlet impedance are owing to friction $(R)$ and to geometry $(M)$, and the total complex impedance caused by an inlet, $Z_I$, can be written as:

$$Z_I = j\omega M + R + Z_S = Z_M + Z_R + Z_S \qquad (4.13)$$

Here, the model is forced at the inlets with the M2 tidal amplitudes and phases for Vineyard Sound (inlet 1) and the Atlantic Ocean (southern inlet), and solves for the voltage, $V_B$ (Figure 4-2B) [analogous to the sea level in the bay in the hydrodynamic model (Figure 4-2A)]. Conservation of current (current in = current out, or volume flux in = volume flux out) is used to solve for $V_B$ with the relation $Z = \rho g \eta / U$:

$$\frac{\eta_B - \eta_1}{Z_{I1}} + \frac{\eta_B - eta_2}{Z_{I2}} + \frac{\eta_B}{Z_C} = 0 \qquad (4.14)$$

yielding:

$$\eta_B = \frac{Z_C Z_{I2} \eta_1 + Z_C Z_{I1} \eta_2}{Z_C Z_{I2} + Z_C Z_{I1} + Z_{I1} Z_{I2}} \qquad (4.15)$$

The impedances are determined by parameters of the system (Equations 4.7 - 4.9 and 4.13) specific to a given inlet system, and $\eta_1$ and $\eta_2$ are the forcing sea levels at each inlet.

## 4.5 Application to the Katama System

In 2011 Katama Inlet was 5 m deep, whereas much of the southern half of Katama Bay was less than 1 m deep (Figure 4-3A,B; Table 4.1). Observations and simulations using the depth-averaged numerical model ADCIRC (Orescanin et al., 2015) and the measured bathymetry (Figure 4-3A) show the amplitude and phase change of the M2 tide from north to south across the system (Figure 4-3). Relative to the amplitude in Edgartown Channel (location A in Figure 4-3A, distance=0 in Figure 4-3C,D), the ADCIRC-simulated amplitude of the M2 component of sea-surface fluctuations decreases slightly across the northern part of the bay (A-E, Figure 4-3C), consistent with the observations (red squares in Figure 4-3C). However, near, and especially within Katama Inlet the tidal amplitude changes by almost 50% (G-J, Figure 4-3C) before leveling off in the ocean outside of the inlet (J-L, Figure 4-3C), suggesting the majority of the evolution occurs near and within Katama Inlet. Similarly, the observed and simulated phases of the M2 tide relative to that at Edgartown remain nearly constant from north to south across most of the bay, decrease rapidly near the southern edge of the flood shoal and across Katama Inlet (F-J, Figure 4-3D), before leveling off in the ocean outside of the inlet (J-L, Figure 4-3D), suggesting the majority of the evolution occurs near and within Katama Inlet.
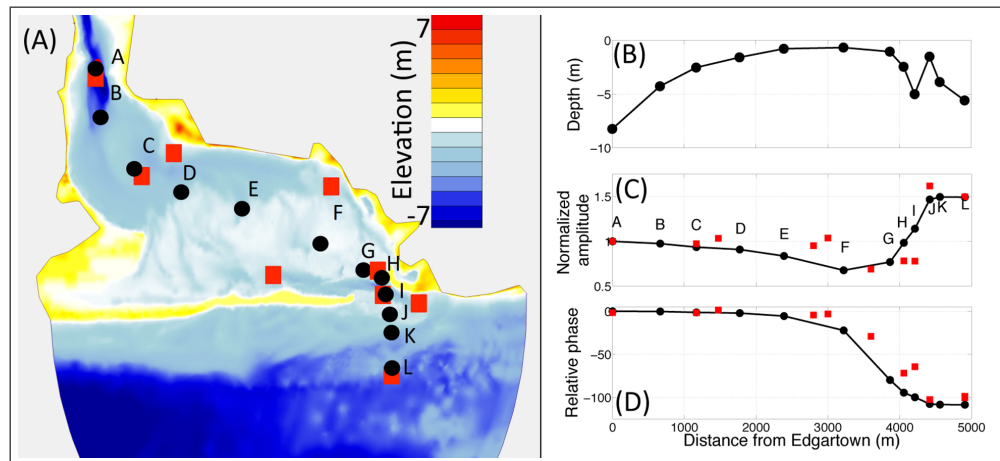


Figure 4-3: A) Contours of elevation (relative to mean sea level) (colors, scale on right) in the Katama system in 2011, and B) the depth versus distance from Edgartown. (C) Amplitudes (normalized by amplitudes at Edgartown) and (D) phases of the M2 tidal constituent (relative to that at Edgartown) versus distance from Edgartown observed (red squares) and simulated with the 2DDI ADCIRC model (black circles and solid curve). The locations of the observations (red squares) and ADCIRC output (A-L) within the inlets and bay are shown in panel A. Katama Inlet is between J and G, where the shallow flood shoal begins.

|  | **2008** | **2011** | **2013** | **2014** |
|---|---|---|---|---|
| **L$_{I2}$ (m)** | 200 | 200 | 800 | 1500 |
| **b$_{I2}$ (m)** | 1000 | 400 | 150 | 150 |
| **h$_{I2}$ (m)** | 6 | 5 | 3 | 2 |

Table 4.1: Dimensions from 2008 are estimated from satellite imagery. Dimensions from 2011-2014 are from satellite imagery and bathymetric surveys. Inlet 1 dimensions are held constant at $L_{I1}$=3500 m, $b_{I1}$=300 m, and $h_{I1}$=8 m. Other input parameters are: $C_{d1}$=0.007, $C_{d2}$= 0.0431, $\rho$=1032 kg/m$^3$, $A_B = 7.5$ x 106 m$^2$, $h_B$=1 m, $a_1$=0.23 m, $a_2$=0.4 m, $\overline{|u_{I1}|}$=0.19 m/s, and $\overline{|u_{I2}|}$=0.76 m/s.

Although the ADCIRC simulations and the observations suggest a change in the tide as it propagates through Katama Inlet and Bay, it is difficult to attribute terms in the governing equations to the effect of the step. However, the effect of the abrupt change between the deeper Katama Inlet and shallower flood shoal can be investigated with the lumped element model (Equation 4.15). The step in depth causes an abrupt change in the tidal phase speed at Katama Inlet, which can be interpreted as mismatched impedance. In contrast, the transition from Edgartown Channel (the inlet that connects Katama Bay to Vineyard sound in the north, A-B, Figure 4-3A) to Katama Bay is more gradual than that at Katama Inlet, and a step is not considered.
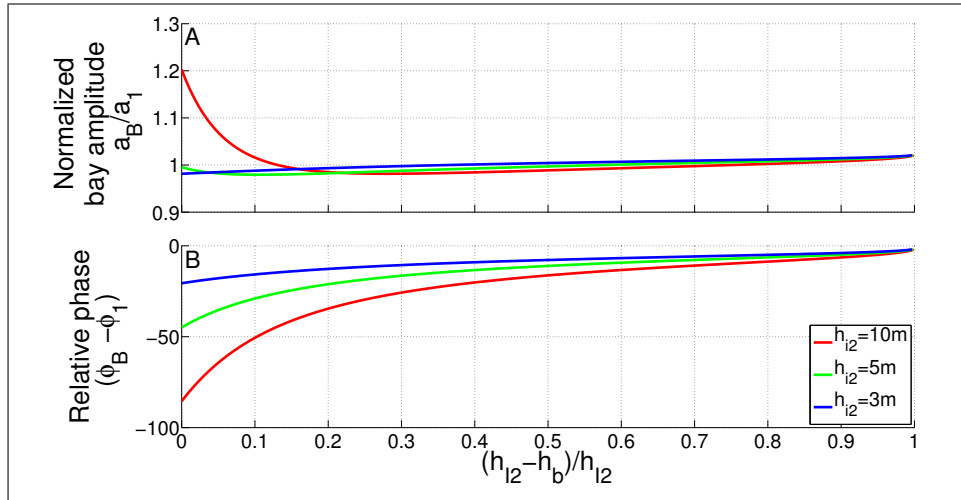


Figure 4-4: Lumped element model simulations of the bay ($h_B = 1$ m) (a) M2 amplitude (normalized by the amplitude of the M2 forcing at Edgartown, $a_1$, the first inlet) and (b) phase (relative to the M2 phase in Edgartown) versus relative step height for three inlet depths (listed in the legend) for the 2011 dimensions. As the relative step size, $(h_I - h_B)/h_I$, approaches 1, the inlet no longer affects the sea level in the bay.

As the relative size of the step between inlet and bay $(h_I - h_B)/h_I$ increases, the influence of the inlet on the bay decreases, and the amplitudes and phases of the M2 tide in the bay approach those of Edgartown Channel (the first inlet) (Figure 4-4). For a system with dimensions similar to Katama, the influence (impedance) of the step increases as the depth of the bay decreases [compare red with blue with green curves in Figure 4-4 for any particular $(h_I - h_B)/h_I$].

The influence of the step decreased as the ratio of inlet length to cross-sectional area at Katama Inlet increased between 2008 and 2013 (Figure 4-5, Table 4.1). In 2008 and 2011, the amplitude and phase of the M2 tide in the bay simulated by the lumped element model without a step [red circles in Figure 4-5, identical to the linearized version of the 1D momentum balance model without a step (blue circles), Orescanin et al. (2014)] is different than simulated by the model with a step (green circles in Figure 4-5). The model with the step (green) more accurately simulates the observations (black symbols in Figure 4-5) in 2011, but all models are similar to the data in 2013, implying the relative importance of the step is reduced, likely owing to the increased importance of friction as the inlet lengthens, narrows, and shoals [Orescanin et al. (2015)].

The lumped element model allows the components of the impedance (Equation 4.15) to be assessed as a function of time (Figure 4-6). Between 2008 and 2011, the Katama Inlet impedance is dominated by the step (green curve in Figure 4-6), but as the inlet evolved between 2011 and 2013, friction (blue curve in Figure 4-6) became as important as the step. The additional lengthening and shoaling of the inlet in 2014 resulted in a much stronger influence of friction (compare blue with green curves in Figure 4-6 for 2014).
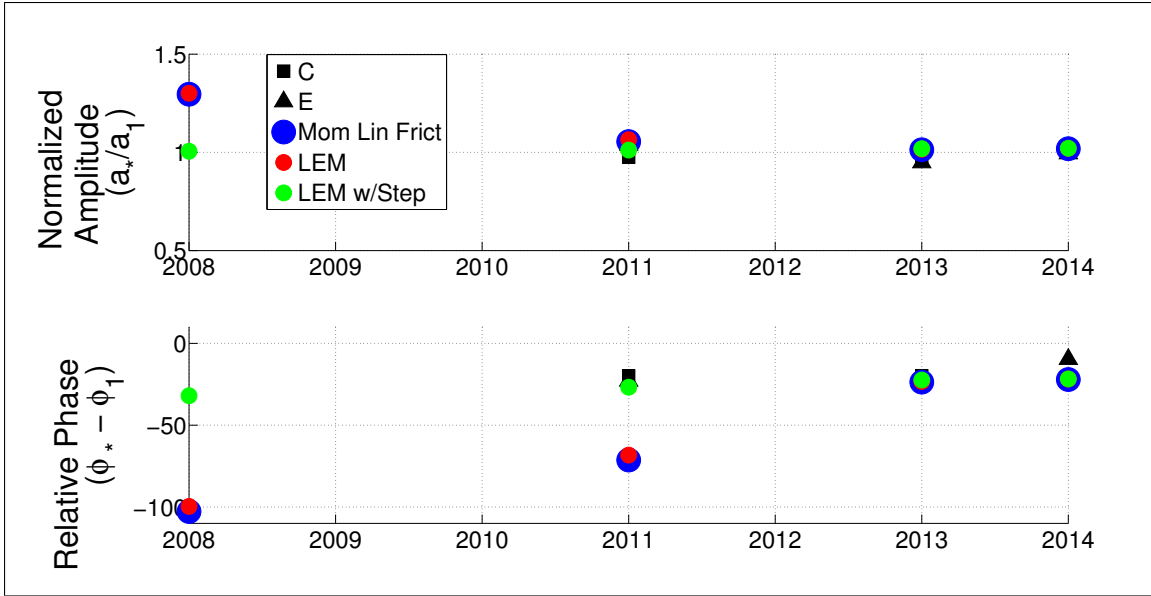
Figure 4-5: A) Amplitude and B) phase of the M2 tidal constituent in the bay relative to those at Edgartown (inlet 1) versus time observed in the north (black square, near "C" in Figure 4-3A) and center (black triangle, near "E" in Figure 4-3A) of the bay, modeled by a 1D momentum balance [Orescanin et al. (2014)] with linearized friction (blue), and the lumped element model with (green) and without (red) a step.
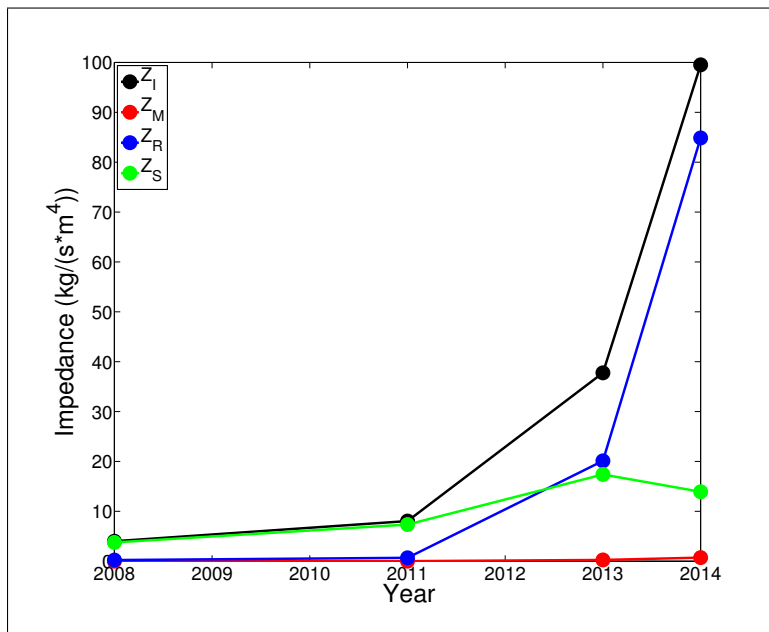


Figure 4-6: Magnitude of the impedance components (Equation 4.13) of Katama Inlet versus time. The total inlet impedance ($Z_I$, black) consists of impedances owing to the physical dimensions of the inlet (inertia, $Z_M$, red), friction ($Z_R$, blue), and the step ($Z_S$, green).

## 4.6 Conclusions

Results from a new lumped element model based on geometrical parameters of a multiple inlet system suggest that the impedance to flow caused by an inlet is a combination of effects from the inertia (mass of water), friction, and a sill or step between the (relatively) deep inlet and the shallow the bay. The sea level response of the bay (and thus currents) can be predicted with this method given geometrical parameters and estimates of a few other parameters (water density, drag coefficients, and a characteristic inlet velocity). By incorporating a shallow flood shoal, represented as a step, the model solutions match observations at the two-inlet system of Katama Bay, Martha's Vineyard, MA. As the step becomes larger or as the ratio of inlet length to cross-sectional area increases, the flow through the inlet is increasingly impeded. The presence of a shallow flood shoal at a wide, short inlet can decrease the importance of an inlet significantly by increasing the impedance. By separating frictional effects from the impedance caused by the step, the lumped element model suggests an increasing importance of friction relative to the importance of the step as Katama Inlet lengthened, narrowed, and shoaled, consistent with observations and previous numerical model results.

# Chapter 5

# Conclusions and Future Work

Evaluating the effects of physical parameters on the hydrodynamics in tidal inlets and back bays, especially multiple tidal inlet systems, allows for an understanding of how each forcing influences the circulation within the bay. This study uses observations, analytical models, and a numerical model (ADCIRC) to address the relative importance of waves, tides, and geometry to sea levels and currents in the two-inlet Katama system, Martha's Vineyard, MA.

Here, it is shown that the influence of waves, tides, and bay bathymetry affect inlet and bay circulation in an evolving multiple tidal inlet system. Specifically, the following new results are presented:

- The momentum from offshore breaking waves enhances flows into inlets, especially during high wave events such as Hurricane Irene. However, in a bay with multiple inlets, the enhanced flow into the bay affects currents much more than bay water levels because water can leave the system via a second inlet. In addition, residual (subtidal) discharge for a 1D momentum balance suggests a southward discharge from Vineyard Sound, through Katama Bay, to the Atlantic Ocean, whereas including wave forcing suggests a northward discharge that is consistent with observations

- The lengthening, shallowing, and rotation of Katama Inlet from 2011 to 2013 resulted in decreased energy within Katama Bay. The relatively small increase in the M4 tidal harmonic and the relatively large increase in the M6 overtide between 2011 and 2013 suggests friction became more important as the inlet lengthened, narrowed and shoaled. Increasing the friction in model simulations with the 2011 bathymetry also

results currents similar to those observed in 2013, consistent with the increasingly important role of friction as the inlet geometry evolved.

- A new lumped element model based on geometric specifications of the inlet(s) and bay(s) is shown to accurately predict the sea level response in Katama Bay if the impedance mismatch at Katama Inlet owing to the shallow flood shoal is considered. The shallowness of the southern Katama Bay relative to the depth of Katama Inlet acts to limit the influence of the inlet on the circulation and distorts the amplitude and phase of the sea level in the bay, resulting in Katama Bay being dominated by Vineyard Sound tides. This model requires knowledge of geometry and estimates of water density, the drag coefficient(s), and characteristic inlet velocities, and uses spatial averaging to provide a simple solution to the sea level response of any inlet-bay system. Thus, any inlet-bay configuration can be predicted using this model with little computational effort yielding accurate first-order predictions. This model has been tested with observations from the Katama Bay system and should be further verified with other inlet systems of differing dimensions and configurations.

## 5.1   Future Work

Even with the contributions presented here, there remain many questions regarding the hydrodynamics of multiple inlet systems. including:

### 5.1.1   Waves and Storms

Changes in climate may result in different frequency and strengths of storms, with subsequent effects on inlets and bays. Specifically, there are many questions related to how storm surge effects multi-inlet systems. For example, storm-induced changes to mean sea level may result in high water levels for extended time periods near one inlet, proving a pressure gradient to drive water toward the other inlet, as was observed in Katama Bay during Hurricane Sandy. In addition, it is not known how these pressure gradients combine with wave-driven overwash to cause a breach in a barrier separating a bay from the ocean.

### 5.1.2 Inlet Impedance

The lumped element model developed in Chapter 4 can help identify several of the processes that affect inlet hydrodynamics. However, this model must be expanded to include nonlinear friction to provide more accurate assessments of systems where friction is important, such as in long, shallow inlets, (e.g., Katama Inlet in 2014). This model may also be expanded to include wave forcing, which would allow for several items in 5.1.1 to be addressed as well.

A long-term research objective is to determine the mechanisms that result in inlet breaching, migration, and closure, especially in a multi-inlet system. With the recent closure of Katama Inlet in April 2015, this system will be an excellent location to monitor the hydrodynamic conditions required for breaching.

# Appendix A

# Inlet Impedance from Back Bay Bathymetry

The general definition of impedance is defined as the ratio of pressure to velocity of a wave, similar to acoustic systems [Dalrymple and Martin (1992); Kinsler et al. (1976)]. In hydrodynamic systems with a wave traveling in one direction (no reflections, etc), hydrostatic pressure, $\rho g h$, is compared with the celerity of the tide, $c = \sqrt{gh}$ to get hydrodynamic impedance:

$$Z_H = \frac{Z}{U} = \frac{\rho g h}{A_I c} = \frac{\rho c}{A_I} = \frac{z_H}{A_I} \tag{A.1}$$

where $P$ is the pressure, $U$ is the volume velocity (discharge), $h$ is the mean water depth, $A_I$ is the cross-sectional area of the inlet, and $z_H = P/u$ is the specific hydrodynamic impedance.

The change in depth between the inlet and bay results in partial transmission and partial reflection of the incoming tide (Figure A-1). The boundary conditions at x = 0 are that the sea levels, $\eta$, and the energy fluxes are the same on both sides.
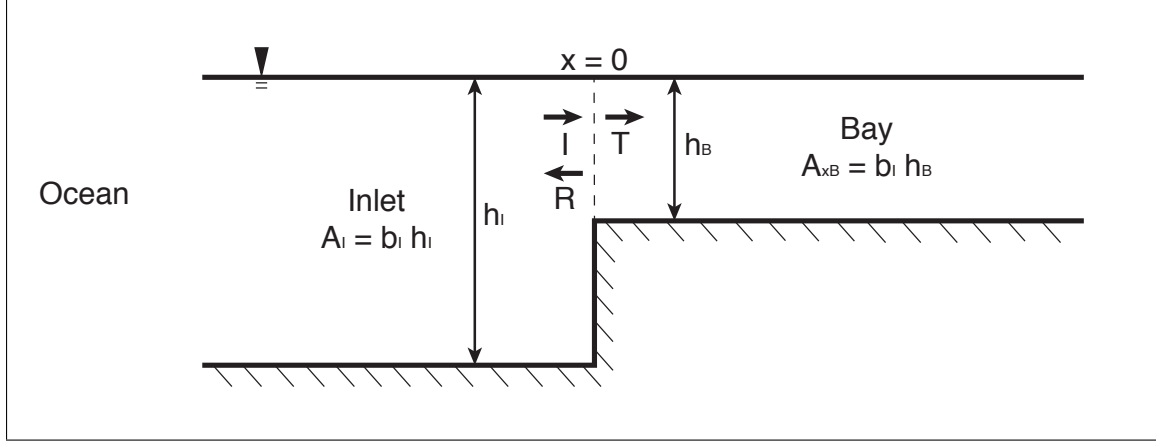
Figure A-1: Schematic of a shallow bay connected to the ocean through a deeper inlet. The arrows labeled $I$, $T$, and $R$, correspond to the incident, transmitted, and reflected waves, respectively. $A_{xB}$ is the cross-sectional area of the bay.

Assuming a generic sinusoidal sea level (can be generalized for multiple frequencies) of the form $\eta_* = a_* sin(\omega t + k_* x)$, where the * subscript can be generalized for the incident, reflected, and transmitted waves, and where $\omega$ is the angular frequency of the incident wave, $t$ is time, and $k_*$ is the wavenumber. For sea level applied at $x = 0$, this is written:

$$\eta_{x=0-} = \eta_{x=0+} \tag{A.2}$$

$$a_i + a_R = a_T \tag{A.3}$$

and for energy flux:

$$\sqrt{gh_I}b_I a_i^2 - \sqrt{gh_I}b_I a_R^2 = \sqrt{gh_B}b_I a_T^2 \tag{A.4}$$

$$(a_i + a_R)(a_i - a_R)\sqrt{h_I} = a_T^2\sqrt{h_B}a_T \tag{A.5}$$

$$a_i - a_R = a_T\sqrt{\frac{h_B}{h_I}} \tag{A.6}$$

Where $b$ is the inlet width and the subscripts $i$ and $I$ refer to the incident wave and inlet location, respectively. Combining A.3 and A.6 above yields:

$$T_o = \frac{a_T}{a_i} = \frac{2\sqrt{h_I}}{\sqrt{h_B} + \sqrt{h_I}} \tag{A.7}$$

$$R_o = \frac{a_R}{a_i} = \frac{\sqrt{h_I} - \sqrt{h_B}}{\sqrt{h_I} + \sqrt{h_B}} \tag{A.8}$$

84

where the subscript 0 refers to $x = 0$. Equations (A.7) and (A.8) describe the transmission and reflection coefficients, respectively, as functions of the depths of the inlet and bay (e.g., Kurkin, 2015). To understand the effect of the reflected wave on the impedance mismatch at the interface $x = 0$, and using the definition, $z = p / u$, divide Equation (A.3) by Equation (A.4), taking note that the velocity here is not a volume velocity and $z$ is the specific impedance, $Z = z / A$. If Equation (A.4) is converted to pressure via $c = \sqrt{gh} = p / z_H$ , the relation between the specific hydrodynamic impedance in the inlet, $z_{HI}$ and bay, $z_{HB}$ becomes:

$$z_{HI}\frac{\rho g(a_i + a_R)}{\rho g(a_i - a_R)} = z_{HB}\frac{\rho g a_T}{\rho g a_T} \tag{A.9}$$

To remove the dependence of the amplitude coefficients, $a_*$, the reflection coefficient, $R_0$, can be defined in terms of impedance:

$$z_{HI}(a_i + a_R) = z_{HB}(a_i - a_R) \tag{A.10}$$

$$a_i(z_{HI} + z_{HB}) = a_T(z_{HB} - z_I) \tag{A.11}$$

$$z_{HI} = z_{HB}\frac{1 - R_o}{1 + R_o} \tag{A.12}$$

Using the definition of $R_0$ from above (Equation A.8) and the definition of hydrodynamic impedance for the bay (Equation A.1), where only a single wave propagates), A.12 becomes:

$$z_{HI} = \rho c_B\frac{1 - \frac{\sqrt{h_I}-\sqrt{h_B}}{\sqrt{h_I}+\sqrt{h_B}}}{1 + \frac{\sqrt{h_I}-\sqrt{h_B}}{\sqrt{h_I}+\sqrt{h_B}}} = \rho c_B\sqrt{\frac{h_B}{h_I}} \tag{A.13}$$

To create an element for the lumped element model defined in Chapter 4 for a multiple inlet system, the impedance difference must be determined. Given the relationship $Z_* = \frac{z_*}{A_*}$ , the excess impedance due to the shallowness of the bay is defined as:

$$Z_S = Z_{HI} - Z_{HB} = \frac{\rho c_B}{h_I b_I}\sqrt{\frac{h_B}{h_I}} - \frac{\rho c_B}{h_B b_I} = \frac{\rho c_B}{b_I h_B}\left(\frac{h_B^{3/2} - h_I^{3/2}}{h_I^{3/2}}\right) \tag{A.14}$$

where $Z_{HI} = \frac{z_{HI}}{A_I}$ is the hydrodynamic impedance in the inlet and $Z_{HB} = \frac{z_{HB}}{A_I}$ is the hydrodynamic impedance of the bay. For $h_I = h_B$, there is no step to impede the flow and $Z_S=0$. As $h_B \to 0$ (for one inlet only), $Z_S \to \infty$, and the flow through the inlet is impeded completely, and the bay mimics the second inlet. As $h_B \to \infty$, the solution, which assumes

shallow water, no longer is valid.

# Bibliography

A. Apotsos, B. Raubenheimer, S. Elgar, and R. Guza. Wave-driven setup and alongshore flows observed onshore of a submarine canyon. *Journal of Geophysical Research*, 113, 2008.

D. Aubrey and G Giese. *Formation and evolution of multiple tidal inlets*, volume 44 of *Coastal and Estuarine Studies*. American Geophysical Union, 1993.

D. G. Aubrey and P. E. Speer. A study of nonlinear tidal propagation in shallow inlet estuarine systems. Part I: Observations. *Estuarine, Coastal, and Shelf Science*, 21(2): 185–205, 1985.

R. A. Bagnold. An approach to the sediment transport problem from general physics. *U.S. Geological Survey Professional Paper*, 422(I), 1966.

J. A. Bailard. An energetics total load sediment transport model for a plane sloping beach. *Journal of Geophysical Research*, 86:10938–10954, 1981.

X. Bertin, A. Fortunato, and A Oliveira. A modeling-based analysis of processes driving wave-dominated inlets. *Continental Shelf Research*, 29:819–834, 2009.

J. O. Blanton, G. Q. Lin, and S. A. Elston. Tidal current asymmetry in shallow estuaries and tidal creeks. *Continental Shelf Research*, 22:1731–1743, 2002.

A. J. Bowen. *Simple models of nearshore sedimentation: Beach profiles and longshore bars.* Geological Survey of Canada Paper 80-10. Geological Survey of Canada, 1980.

L. C. Breaker, W. W. Broenkow, W. E. Watwon, and Y.-H. Jo. Tidal and nontidal oscillations in Elkhorn Slough, CA. *Estuaries and Coasts*, 31(2):239–257, 2008.

W. W. Broenkow and L. C. Breaker. A 30-year history of tide and current measurements in Elkhorn Slough, California (November 18, 2005). *Scripps Institution of Oceanography Library*, Paper 8, 2005.

R. L. Brouwer, H. M. Schuttelaars, and P. C. Roos. Modelling the influence of spatially varying hydrodynamics on the cross-sectional stability of double inlet systems. *Ocean Dynamics*, 63:1263–1278, 2013.

W. Brown and R. Trask. A study of tidal energy dissipation and bottom stress in an estuary. *Journal of Physical Oceanography*, 10:1742–1754, 1980.

P Bruun. *Stability of tidal inlets: Theory and engineering.* Elsevier, 1978.

P. Bruun and J. Adams. Stability of tidal inlets: Use of hydraulic pressure for channel and bypassing stability. *Journal of Coastal Research*, 4:687–701, 1988.

A Campbell, J. Simpson, and G Allen. The dynamical balance of flow in the Menai Strait. *Coastal and Shelf Science*, 46:449–455, 1998.

C. Chen, H. Huang, R. Beardsley, Q. Xu, R. Limeburner, G. Cowles, Y. Sun, J. Qi, and H. Lin. Tidal dynamics in the Gulf of Maine and New England Shelf: An application of FVCOM. *Journal of Geophysical Research*, 116:C12010, 2011.

R. A. Dalrymple and P. A. Martin. Perfect boundary conditions for parabolic water-wave models. *Procedings of the Royal Society of London A*, 437:41–54, 1992.

H. E. De Swart and N. D. Volp. Effects of hypsometry on the morphodynamic stability of single and multiple tidal inlet systems. *Journal of Sea Research*, 74:35–44, 2012.

G. Dodet, X. Bertin, N. Bruneau, A. Fortunato, A. Nahon, and A. Roland. Wave-current interactions in a wave-dominated tidal inlet. *Journal of Geophysical Research*, 118:1587–1605, 2013.

T. Drake and J. Calantoni. Discrete particle model for sheet flow sediment transport in the nearshore. *Journal of Geophysical Research*, 106:19859, 2001.

J. Dronkers. Tidal asymmetry and estuarine morphology. *Netherlands Journal of Sea Research*, 20:117–131, 1986.

M. Easton, D. Woolf, and P. Bowyer. The dynamics of an energetic tidal channel, the Pentland Firth, Scotland. *Continental Shelf Research*, 48:50–60, 2012.

S. Elgar and R. T. Guza. Observations of bispectra of shoaling surface gravity waves. *Journal of Fluid Mechanics*, 161:425–448, 1985.

S. Elgar and B. Raubenheimer. Currents in a small channel on a sandy tidal flat. *Continental Shelf Research*, 31:9–14, 2010.

A. B. Fortunato and A. Oliveira. Influence of intertidal flats on tidal asymmetry. *Journal of Coastal Research*, 21:1062–1067, 2005.

C. T. Friedrichs and D. G. Aubrey. Non-linear tidal distortion in shallow water well-mixed estuaries: a synthesis. *Estuarine, Coastal, and Shelf Science*, 27(5):521–545, 1988.

C. T. Friedrichs, D. R. Lynch, and D. G. Aubrey. Velocity asymmetries in frictionally dominated tidal embayments: Longitudinal and lateral variability. In D. Prandle, editor, *Dynamics and Exchanges in Estuaries and the Coastal Zone, Coastal and Estuarine Studies*, volume 40, pages 276–312. American Geophysical Union, Washington, D. C., 1992.

W. R. Geyer and P. MacCready. The estuarine circulation. *Annual Review in Fluid Mechanics*, 46:175–197, 2014.

G Giese and D. Jay. Modeling estuary energetics of the Colombia River estuary. *Estuarine, Coastal, and Shelf Science*, 29:549–571, 1989.

Lewis M. Haupt. Fire Island Inlet. Is it moving east or west, and at what rate? *Journal of the Franklin Institute*, 127(4):249–254, 1889.

J. Hench and R. Luettich. Transient tidal circulation and momentum balances at a shallow inlet. *Journal of Physical Oceanography*, 33:913–932, 2003.

A. Herman. Numerical modelling of water transport processes in partially-connected tidal basins. *Coastal Engineering*, 54:297–320, 2007.

F. Hoefel and S. Elgar. Wave-induced sediment transport and sandbar migration. *Science*, 299:1885–1887, 2003.

D. Jay. Green's law revisited: Tidal long-wave propagation in channels with strong topography. *Journal of Geophysical Research*, 96:20,585–20,598, 1991.

G. H. Keulegan. Tidal flow in engrances; water-level fluctuations of basins in communication with seas. *Committee on Tidal Hydraulics (Army), Washington D.C.*, CTH Technical Bulletin-14, 1967.

S. Kim, C. Friedrichs, J. Maa, and L. Wright. Estimating bottom stress in tidal boundary layer from acoustic Doppler velocimeter data. *Journal of Hydraulic Engineering*, 126: 499–506, 2000.

Y. C. Kim and E. J. Powers. Digital bispectral analysis and its application to nonlinear wave interactions. *IEEE Transactions in Plasma Science*, 7:120–131, 1979.

L. E. Kinsler, A. B. Frey, A. B. Coppens, and J. V. Sanders. *Fundamentals of Acoustics.* John Wiley & Sons, Inc., Hoboken, NJ, 1976.

N. C. Kraus and A. Militello. Hydraulic study of multiple inlet system: East Matagorda Bay, Texas. *Journal of Hydraulic Engineering*, 125(3):224–232, 1999.

A. A. Kurkin. Transformation of surface waves over a bottom step. *Izvestiya, Atmospheric and Oceanic Physics*, 51(2):214–223, 2015.

W. Large and S. Pond. Open ocean momentum flux measurements in moderate to strong winds. *Journal of Physical Oceanography*, 11:324–336, 1981.

C. Le Provost. *Generation of overtides and compound tides, review.* John Wiley & Sons, Inc., New York, New York, 1991.

L LeConte. Discussion on the paper, "Notes on the improvement of river and harbor outlets in the United States" by D. A. Watt. *Transactions of ASCE*, 55:306–308, December 1905.

S. Lentz, R. Guza, S. Elgar, F. Feddersen, and T. Herbers. Momentum balances on the North Carolina inner shelf. *Journal of Geophysical Research*, 104:18,205–18,226, 1999.

M. Longuet-Higgins. Longshore currents generated by obliquely incident sea waves. *Journal of Geophysical Research*, 75:6778–6789, 1970.

M. Longuet-Higgins and R. Stewart. Radiation stresses in water waves: A physical discussion with applications. *Deep Sea Research*, 11:529–562, 1964.

R. A. Luettich and J. J. Westerink. A solution for the vertical variation of stress, rather than velocity in a three-dimensional circulation model. *International Journal for Numerical Methods in Fluids*, 12:911–928, 1991.

R. A. Luettich, J. J. Westerink, and N. W. Scheffner. ADCIRC: An advanced three-dimensional model for shelves, coasts, and estuaries. report 1: Theory and methodology of ADCIRC 2DDI and ADCIRC 3-DL. *Dredging Research Program Tech. Rep. DRP-92-6, Coastal Engineering Research Center, U.S. Army Corps of Engineers, Waterways Experiment Station*, page 141, 1992.

L. R. Maas. On the nonlinear Helmholtz response of almost-enclosed tidal basins with sloping bottoms. *Journal of Fluid Mechanics*, 349:361–380, 1997.

L. R. Maas and A. Doelman. Chaotic tides. *Journal of Physical Oceanography*, 32:870–890, 2002.

P. MacCready and W. R. Geyer. Advances in estuarine physics. *Annual Review of Marine Science*, 2010.2:35–58, 2010.

M. Malhadas, P. Leitao, A. Silva, and R. Neves. Effect of coastal waves on sea level in Obidos Lagoon, Portugal. *Continental Shelf Research*, 29:1240–1250, 2009.

A. Masuda and Y.-Y. Kuo. A note on the imaginary part of bispectra. *Deep Sea Research*, 28:213–222, 1981.

J. W. Miles. Resonant response of harbours: an equivalent-circuit analysis. *Journal of Fluid Mechanics*, 46(02):241–265, 1971.

J. W. Miles. Harbor seiching. *Annual Review in Fluid Mechanics*, 6(1):17–33, 1974.

J. W. Miles and Y. K. Lee. Helmholtz resonance of harbours. *Journal of Fluid Mechanics*, 67(03):445–464, 1975.

I. Nezu and W. Rodi. Open-channel flow measurements with a laser Doppler anemometer. *Journal of Hydraulic Engineering*, 112(5):335–355, 1986.

R. L. Nichols and A. F. Marson. Shoreline changes in Rhode Island produced by hurricane of September 21, 1938. *Geological Society of America Bulletin*, 50(9):1357–1370, 1939.

N. J. Nidzieko. Tidal asymmetry in estuaries with mixed semidiurnal/diurnal tides. *Journal of Geophysical Research*, 115(C08006), 2010.

N. J. Nidzieko and D. Ralston. Tidal asymmetry and velocity skew over tidal flats and shallow channels within a macrotidal river delta. *Journal of Geophysical Research*, 117 (C03001), 2012.

M. P. O'Brien. Estuary tidal prism related to entrance areas. *Civil Engineering*, 1(8): 738–739, 1931.

M. P. O'Brien. Equilibrium flow areas of inlets on sandy coasts. *Journal of the Waterways, Harbors, and Coastal Engineering Division of ASCE*, 95(1):43–52, 1969.

M. P. O'Brien and R. R. Clark. Hydraulic constants of tidal entrances. *Coastal Engineering Proceedings*, 1(14), 1974.

J. G. Ogden. Shoreline changes along the southeastern coast of Martha's Vineyard, Massachusetts for the past 200 years. *Quarternary Research*, 4:496–508, 1974.

M. Olabarrieta, J. Warner, and N. Kumar. Wave-current interaction in Willipa Bay. *Journal of Geophysical Research*, 116:C12014, 2011.

M. Orescanin, B. Raubenheimer, and S. Elgar. Observations of wave effects on inlet circulation. *Continental Shelf Research*, 82:37–42, 2014.

M. M. Orescanin, S. Elgar, and B. Raubenheimer. Changes in bay circulation in an evolving multiple inlet system. *Continental Shelf Research*, in press, 2015.

A. Pacheco, Ó. Ferreira, J. J. Williams, E. Garel, A. Vila-Concejo, and J. A. Dias. Hydrodynamics and equilibrium of a multiple-inlet system. *Marine Geology*, 274(1):32–42, 2010.

B. B. Parker. *The relative importance of the various nonlinear mechanisms in a wide range of tidal interactions (Review).* John Wiley & Sons, Inc., New York, 1991.

R. Pawlowicz, B. Beardsley, and S. Lentz. Classical tidal harmonic analysis including error estimates in MATLAB using T_TIDE. *Computers and Geosciences*, 28:929–937, 2002.

A. Pierce. *Acoustics: An Introduction to its physical principles and applications.* Acoustical Society of America, 1989.

D. Prandle. *Tides in estuaries and embayments.* John Wiley & Sons, Inc., New York, 1991.

J. Proudman. *Dynamical Oceanography.* Methuen, London, 1953.

P. Salles, G. Voulgaris, and D. Aubrey. Contribution of nonlinear mechanisms in the persistence of multiple tidal inlet systems. *Estuarine, Coastal, and Shelf Science*, 65:475–491, 2005.

K. Shearman and S. Lentz. Observations of tidal variability on the New England shelf. *Journal of Geophysical Research*, 109:C06010, 2004.

P. E. Speer and D. G. Aubrey. A study of nonlinear tidal propagation in shallow inlet estuarine systems. Part II: Theory. *Coastal and Shelf Science*, 21(2):207–224, 1985.

P. E. Speer, D. G. Aubrey, and C. T. Friedrichs. *Nonlinear hydrodynamics of shallow tidal inlet/bay systems.* John Wiley & Sons, Inc., New York, 1991.

E. V. Stanev, G. Flöser, and J. O. Wolff. First-and higher-order dynamical controls on water exchanges between tidal basins and the open ocean. a case study for the East Frisian Wadden Sea. *Ocean Dynamics*, 53(3):146–165, 2003.

C. Stevens, P. Sutton, M. Smith, and R. Dickson. Tidal flows in Te Aumiti (French Pass), South Island, New Zealand. *New Zealand Journal of Marine and Freshwater Research*, 42:451–464, 2008.

T. Stevenson. *Design and construction of harbours.* Adam and Charles Black, Edinburgh, 3rd edition, 1886.

G. T. Terra, W. J. van de Berg, and L. R. M. Maas. Experimental verification of Lorentz' linearization procedure for quadratic friction. *Fluid Dynamics Research*, 36:175–188, 2005.

E. Thornton, J. MacMahan, S. Elgar, C. Gon, and A. Reniers. Tidal wave reflection and asymmetry in a short estuary. *Journal of Geophysical Research*, submitted.

J. van de Kreeke, J. Brouwer, T. Zitman, and H. Schuttelaars. The effect of a topographic high on the morphological stability of a two-inlet system. *Coastal Engineering*, 55:319–332, 2008.

S. M. Van Leeuwen and H. E. De Swart. Intermediate modelling of tidal inlet systems: spatial asymmetries in flow and mean sediment transport. *Continental Shelf Research*, 22 (11):1795–1810, 2002.

A. Wargula, B. Raubenheimer, and S. Elgar. Wave-driven along-channel subtidal flows in a well-mixed ocean inlet. *Journal of Geophysical Research*, 119(5):2987–3001, 2014.

A. F. Waterhouse, A. Valle-Levinson, and C. D. Winant. Tides in a system of connected estuaries. *Journal of Physical Oceanography*, 41(5):946–959, 2011.

G. Wheless and A. Valle-Levinson. A modeling study of tidally driven estuarine exchange through a narrow inlet onto a sloping shelf. *Journal of Geophysical Research*, 101:25,675–25,687, 1996.